# Using observed urban $NO_x$ sinks to constrain VOC reactivity and the ozone and radical budget in the Seoul Metropolitan Area

Benjamin A. Nault[1,2,*], Katherine R. Travis[3], James H. Crawford[3], Donald R. Blake[4], Pedro Campuzano-Jost[5], Ronald C. Cohen[6], Joshua P. DiGangi[3], Glenn S. Diskin[3], Samuel R. Hall[7], L. Gregory Huey[8], Jose L. Jimenez[5], Kyung-Eun Kim[9], Young Ro Lee[8,a], Isobel J. Simpson[4], Kirk Ullmann[7], Armin Wisthaler[10,11]

[1]CACC, Aerodyne Research, Inc., Billerica, MA, USA
[2]Department of Environmental Health and Engineering, Johns Hopkins University, Baltimore, MD, USA
[3]NASA Langley Research Center, Hampton, VA, USA
[4]Department of Chemistry, University of California, Irvine, CA, USA
[5]CIRES and Department of Chemistry, University of Colorado, Boulder, CO, USA
[6]Department of Chemistry, University of California, Berkeley, CA, USA
[7]Atmospheric Chemistry Observations & Modeling Laboratory, NCAR, Boulder, CO, USA
[8]School of Earth & Atmospheric Sciences, Georgia Institute of Technology, Atlanta, GA, USA
[9]School of Environmental Sciences and Environmental Engineering, Gwangju Institute of Science and Technology, Gwangju, South Korea
[10]University of Oslo, Oslo, Norway
[11]University of Innsbruck, Innsbruck, Austria

[a]Now at Division of Geological and Planetary Sciences, California Institute of Technology, Pasadena, CA, USA

[*]Corresponding author:
Email: bnault@aerodyne.com, bnault1@jh.edu

*For ACP*

**Abstract**

Ozone ($O_3$) is an important secondary pollutant that impacts air quality and human health. Eastern Asia has high regional $O_3$ background due to the numerous sources and increasing and rapid industrial growth, which impacts the Seoul Metropolitan Area (SMA). However, SMA has also been experiencing increasing $O_3$ driven by decreasing $NO_x$ emissions, highlighting the role of local, in-situ $O_3$ production on SMA. Here, comprehensive gas-phase measurements collected on the NASA DC-8 during the NIER/NASA Korea United States-Air Quality (KORUS-AQ) study are used to constrain the instantaneous $O_3$ production rate over the SMA. The observed $NO_x$ oxidized products support the importance of non-measured peroxy nitrates (PNs) in the $O_3$ chemistry in SMA, as they accounted for ~49% of the total PNs. Using the total measured PNs (ΣPNs) and alkyl and multifunctional nitrates (ΣANs), unmeasured volatile organic compound (VOC) reactivity (R(VOC)) is constrained and found to range from 1.4 – 2.1 $s^{-1}$. Combining the observationally constrained R(VOC) with the other measurements on the DC-8, the instantaneous net $O_3$ production rate, which is as high as ~10 ppbv $hr^{-1}$, along with the important sinks of $O_3$ and radical chemistry, are constrained. This analysis shows that ΣPNs play an important role in both the sinks of $O_3$ and radical chemistry. Since ΣPNs are assumed to be in steady-state, the results here highlight the role ΣPNs play in urban environments in altering net $O_3$ production, but ΣPNs can potentially lead to increased net $O_3$ production downwind due to their short lifetime (~1 hr). The results provide guidance for future measurements to identify the missing R(VOCs) and ΣPNs production.

**Short Summary**

Ozone ($O_3$) is a pollutant formed from the reactions of gases emitted from various sources. In urban areas, the density of human activities can increase the $O_3$ formation rate ($P(O_3)$); thus, impact air quality and health. Observations collected over Seoul, South Korea, are used to constrain $P(O_3)$. A high local $P(O_3)$ was found; however, local $P(O_3)$ was partly reduced due to compounds typically ignored. These observations also provide constraints for unmeasured compounds that will impact $P(O_3)$.

## 1. Introduction

Representing global and urban tropospheric ozone ($O_3$) in chemical transport models (CTMs) is still challenging due to uncertainty in physical and chemical processes that control the $O_3$ budget (Archibald et al., 2020). One area of uncertainty is underestimated urban volatile organic compounds (VOCs) emissions (von Schneidemesser et al., 2023), which arise from a large number of sources, including some that are very hard to quantify (e.g., cooking and chemical products) (e.g., McDonald et al., 2018; Simpson et al., 2020). Intensive research is also ongoing as to why $O_3$ is increasing in recent years in urban areas, even with reductions in combustion emissions (Colombi et al., 2023; e.g., Lyu et al., 2017). This $O_3$ impacts the large populations in urban areas with harmful health effects, including premature mortality (e.g., Cohen et al., 2017).

Tropospheric $O_3$ production is driven by the catalytic cycling of nitrogen oxides ($NO_x$ = NO + $NO_2$) fueled by the photoxidation of VOCs, both of which can come from anthropogenic emissions. The chemistry producing $O_3$ is described in R1 – R6 in Table 1. During daylight hours, VOCs are oxidized by OH (or undergo photolysis) to form an organic peroxy radical ($RO_2^{\cdot}$) in R1a (R1b). If the $RO_2^{\cdot}$ then proceeds through R2a, at least two $O_3$ molecules are produced. The first $O_3$ molecule is formed by the photolysis of $NO_2$ and the reaction of $O(^3P)$ with oxygen (R3 – R4). The second $O_3$ molecule is formed through the reaction of the alkoxy radical ($RO^{\cdot}$) with oxygen to form the hydroperoxyl radical ($HO_2$) (R5), which goes on to react with NO to produce $NO_2$ (R6) and the subsequent reactions described above (R3 – R4). However, some fraction of the time, depending on the number of carbons and functional group (e.g., Espada and Shepson, 2005; Perring et al., 2013; Yeh and Ziemann, 2014), alkyl or multifunctional nitrates (ANs ≡ $RONO_2$) are formed (R2b). The fraction of reactions to form ANs is described by the branching ratio, α. Reaction R2b has been shown to impact $O_3$ production, depending on the types of VOC emitted,

by reducing the fraction of $NO_2$ that photolyzes to form $O_3$ in source regions (R3 – R4) (Farmer et al., 2011). As α is a function of the individual VOC's carbon backbone and functional group (e.g., Perring et al., 2013), any uncertainty related to primary VOC emissions and secondary chemistry will directly impact the ability to describe urban $O_3$ production.

One important subclass of VOCs are aldehydes (RCHO), which can either be directly emitted or produced via photooxidation of VOCs (de Gouw et al., 2018; Mellouki et al., 2015; Wang et al., 2022; Yuan et al., 2012). The photooxidation of the aldehyde (R7) in the presence of $NO_x$ can either form acyl peroxy nitrates (R8, PNs = $R(O)O_2NO_2$) or an organic peroxy radical ($RO_2^{\cdot}$) (R9). The competition between R8 to form PNs versus R9 to form $RO_2^{\cdot}$ depends on the NO-to-$NO_2$ ratio (Nihill et al., 2021). Further, R8 is in thermodynamic equilibrium due to the weak bond strength between the acyl peroxy radical ($R(O)O_2^{\cdot}$) and $NO_2$. Thus, formation of PNs pose only a temporary loss of $NO_2$. Finally, it has been observed that aldehydes with longer carbon backbones (e.g., C8s and C9s) from various anthropogenic activities, such as cooking (Coggon et al., 2024; Rao et al., 2010), may have mixing ratios as high as aldehydes typically quantified in field experiments (acetaldehyde and propaldehyde). However, there is larger uncertainty associated with these higher aldehydes in their fate to produce both PNs and ANs (e.g., Hurst Bowman et al., 2003). Missing both these emissions and subsequent chemistry would impact estimates of urban $O_3$ chemistry.

The fraction of $RO_2^{\cdot}$ forming ANs in R2b and the fraction of $R(O)O_2^{\cdot}$ forming PNs in R8 alter the instantaneous $O_3$ production ($P(O_3)$) by removing $NO_2$ and/or the radical species. This is further shown in Figure S1, where an analytical equation to describe R1 – R6 (Farmer et al., 2011), is used to explore how changes in the VOC reactivity (R(VOC)), radical production ($P(HO_x)$), and ANs production and branching ratio, α (R2b), impact the instantaneous $P(O_3)$ (see Sect. S1 for the

analytical equation and description). Any changes in $P(HO_x)$, R(VOC), and/or α will impact both the instantaneous $P(O_3)$ as well as the $NO_x$ mixing ratio corresponding to the maximum $P(O_3)$. As these parameters are generally interconnected, investigating all three is important to understand the sources and control of instantaneous $P(O_3)$. Further, R7 – R9 are not included in this traditional description of the analytical equation, as it is assumed PNs are in steady-state (Farmer et al., 2011). Thus, if PNs are not in steady-state, their role in altering $P(O_3)$ may be underestimated.

Increasing surface $O_3$ is a concern throughout East Asia, including South Korea (Colombi et al., 2023; Gaudel et al., 2018; Kim et al., 2021; Yeo and Kim, 2021). The emissions associated with industry and other anthropogenic activities and the associated photochemistry have impacted regional air quality, leading to high $O_3$ backgrounds that can impact a country's ability to achieve reduced $O_3$ exposure for new air quality standards (e.g., Colombi et al., 2023). However, local emissions and photochemistry still play an important role. For example, during the Korea-United States Air Quality (KORUS-AQ) campaign, it was observed between morning and afternoon in the Seoul Metropolitan Area (SMA), $O_3$ increased by ~20 parts per billion by volume (ppbv) over a background concentration of over 75 ppbv (Crawford et al., 2021). Thus, an understanding of the variables highlighted in Figure S1 are necessary to control both local and regional $P(O_3)$.

One tool typically used to understand the role of regional $O_3$ and transported $O_3$ on local $O_3$ and impacts of local emission controls on $O_3$ are CTMs. As shown in Park et al. (2021), for the SMA, CTMs typically underestimate the observed $O_3$ and formaldehyde. While the low $O_3$ could be partially related to underestimated transport (e.g., Seo et al., 2018) or resolution of the CTM (e.g., Jo et al., 2023; Park et al., 2021), the low bias also observed for modeled formaldehyde indicates overall (a) too little VOCs and thus too low R(VOC) (Brune et al., 2022; H. Kim et al., 2022), (b) missing photochemical products from missing VOCs, including oxygenated VOCs

(OVOCs) that contribute to P($HO_x$) (Brune et al., 2022; H. Kim et al., 2022; Lee et al., 2022; Wang et al., 2022), and (c) likely missing PNs and ANs from the underestimated VOCs related to the underestimated R(VOC) (Lee et al., 2022; Park et al., 2021). Missing (a) – (c) will bias the instantaneous P($O_3$) (Figure S1), impacting the ability to investigate what policies should be implemented to reduce $O_3$.

To better understand what controls the instantaneous P($O_3$) over SMA, observations collected on the NASA DC-8 during KORUS-AQ are used to constrain the three variables highlighted in Figure S1—R(VOC), $HO_x$ production and loss, and ANs and PNs production. Observational constraints on these three parameters provide a means to investigate the instantaneous P($O_3$) over SMA and the major classes of contributors to $O_3$ and $HO_x$ production and loss. These results are discussed and placed into the context of improving our knowledge about $O_3$ production in an urban environment.

## 2. Methods and Data Description

### 2.1 KORUS-AQ and DC-8 Descriptions

The KORUS-AQ campaign was a multi-national project that was conducted in May – June, 2016, led by South Korea's National Institute of Environmental Research (NIER) and United States National Aeronautics and Space Administration (NASA). The project was conducted in South Korea and the surrounding seas with numerous airborne platforms, research vessels, and ground sites (Crawford et al., 2021). The study here focuses on the observations collected on the NASA DC-8.

The instrument payload, flights, and observations have been described in other studies (Brune et al., 2022; Crawford et al., 2021; Lee et al., 2022; Schroeder et al., 2020). Briefly, the

DC-8 was stationed at Osan Air Force Base, Pyeongtaek, South Korea, which is approximately 60 km south of Seoul. A total of 20 research flights were conducted with the DC-8. Part of each research flights included a stereo-route in the SMA in the morning (~09:00 local time), midday (~12:00 local time), and afternoon (~15:00 local time), which included a missed approach over Seoul Air Base (< 15 km from Seoul city center) and a fly-over of the Olympic Park and Taehwa Forest Research sites (Figure 1). A total of 55 descents over Olympic Park and 53 spirals over Taehwa Forest Research site were conducted (Crawford et al., 2021). Only observations from the DC-8 after 11:00 local time are used here to ensure that the boundary layer has grown and stabilized and to minimize any influence from residual layer mixing into the boundary layer and/or titration of $O_3$ by NO (R10). We analyze data collected below 2 km and between 127.10 – 127.67°E and 37.22 – 37.69°N to focus on the boundary layer in the SMA without influence from industrial emissions along the western South Korean coast (Crawford et al., 2021).

During KORUS-AQ, four different meteorological periods, as described by Peterson et al. (2019), impacted the region. These periods included a Dynamic period from 1 – 16 May, where there were a series of frontal passages; a Stagnant period from 17 – 22 May, where it was dry, clear, and stagnant; Transport/Haze period from 25 – 31 May, where long-range transport and hazy conditions with high humidity and cloud cover prevailed; and, a Blocking period from 1 – 7 June, where a high pressure ridge is located to an area north of lower pressure, which can preclude significant changes in synoptic meteorology and results in occasional stagnant conditions/minimal pollution transport (Peterson et al., 2019). However, as discussed in Sect. 3.2, conditions did not impact the general trends and chemistry and thus the whole campaign has been analyzed together.

The observations used for the analysis are shown in Table 2, along with the associated references. The 1-min merged data from the DC-8 is used here (KORUS-AQ Science Team, 2023).

For data missing due to frequency of measurements (e.g., VOCs from WAS), data was filled in a similar approach as Schroeder et al. (2020), in that VOCs with missing data were filled by the linear relationship of that VOC with VOCs measured more frequently. This step was necessary for the observations used in the diel steady-state calculations described in Sect. 2.2. Note, the TD-LIF $NO_2$ (see Table 2) was used throughout this study and discussed in Sect. S2 and Figure S2 – S4 as it generally agreed better with steady-state calculated $NO_2$-to-NO ratios and steady-state $NO_2$ than the chemiluminescence $NO_2$. Further, though PBzN was measured by GT-CIMS (Table 2), it is not compared with calculated PBzN from F0AM (Sect. 2.2) as it may be underestimated due to possible inlet losses, as discussed in Zheng et al. (2011).

## 2.2 F0AM Box Model Diel Steady-State Calculations for Missing Reactivity and Peroxynitrate Budget Analysis

We use the F0AM box model (Wolfe et al., 2016) with chemistry from the MCMv3.3.1 (Jenkin et al., 2015) to simulate production of PNs and formaldehyde using 1-min merged data, as described in Sect. 2.1. As in Schroeder et al. (2020), we simulate each 1-min merged aircraft observation through the full diurnal solar cycle (i.e., diel steady-state) until the diurnal cycle for each unconstrained species reaches convergence within 1%. These unconstrained species, such as formaldehyde, $NO_2$, and OH, are then evaluated to ensure consistency between F0AM model and aircraft observations. We constrain concentrations of NO, $O_3$, $H_2O_2$, $HNO_3$, CO, $CH_4$, $H_2$, PAN, PPN, and all measured or estimated VOCs given in Table 2 and Table S1 to calculate $HO_2$, all organic peroxy and acyl peroxy radicals, and unmeasured PNs. To calculate the PAN and PNs budget, we allow the model to freely calculate $NO_2$, formaldehyde, acetaldehyde, and all PNs, including PAN and PPN, for when calculating the budget of PNs. We use a dilution constant of 12

hours, according to Brune et al. (2022). Model evaluation is discussed in Sect. 3.4. The contribution of individual VOCs to PAN was calculated by reducing precursor VOCs by 20% and multiplying the resulting impact on the peroxy acetyl radical ($CH_3C(O)O_2^{\cdot}$) by 5. Other acyl peroxy nitrates (higher PNs) are lumped into categories based on their primary precursor species from Table S2, species currently typically measured (e.g., PPN) or contributes a large fraction of the total higher PNs budget (greater than >2%; e.g., PHAN and MPAN).

Note, the reason PAN and PPN were constrained were due to uncertainties in the thermal lifetime, temperature history, and dilution rate used in F0AM, which had larger impacts on the $CH_3C(O)O_2^{\cdot}$ and PAN than on other unconstrained compounds (e.g., OH and formaldehyde and not shown; Brune et al. (2022)).Part of this larger impact is due to $CH_3C(O)O_2^{\cdot}$ being one of the most abundant radicals and one of the final radical products in the oxidation of numerous compounds (e.g., Jenkin et al., 2015). We do not expect these uncertainties to impact the higher PNs as (a) there are less precursors to form them compared to PAN and (b) they are expected to have higher thermal stability compared to PAN due to longer carbon backbone (Kabir et al., 2014).

## 2.3 Calculation of Instantaneous Ozone and $HO_x$ Production and Loss

An experimental budget for the production and loss of $O_x$ ($O_x = O_3 + NO_2$) and $HO_x$ ($HO_x = OH + HO_2 + RO_2^{\cdot} + R(O)O_2^{\cdot}$) is described here. $NO_2$ and $O_3$ are combined to reduce any potential impact from titration via $O_3$ reaction with NO (R10). The budget analysis includes field-measured quantities (mixing ratios and photolysis rates, Table 2), results from F0AM (Sect. 2.2), estimated missing R(VOC) (Sect. 3.2) and published kinetic rate constants (see Table 1 for references). The rate of production or destruction is calculated with the following equations (Eq. 1 – 7) below. Note, these equations differ from Schroeder et al. (2020) in that (a) ANs and PNs chemistry are explicitly

included and (b) the reaction of $O_3$ with alkenes is excluded as this reaction contributed a minor loss to $O_3$ (< 1%).

$$P_{O_x} = \sum_i (1-\alpha_{ieff}) k_{RO_{2,i}+NO} [RO_{2,i}^{\cdot}][NO] + k_{HO_2+NO}[HO_2][NO] \quad (1)$$

$$L_{O_x} = k_{NO_2+OH}[NO_2][OH] + k_{O_3+OH}[O_3][OH] + f \times j_{O^1D}[O_3] + k_{HO_2+O_3}[HO_2][O_3] + net(PNs) \quad (2)$$

$$net(PNs) = \beta k_{R(O)O_2^{\cdot}+NO_2}[R(O)O_2^{\cdot}][NO_2] - (1-\beta) k_{decomposition}[PNs] \quad (3)$$

$$\beta = \frac{k_{RC(O)O_2+NO_2}[NO_2]}{k_{RC(O)O_2+NO_2}[NO_2] + k_{RC(O)O_2+NO}[NO]} \quad (4)$$

$$P(HO_x) = 2f \times j_{O^1D}[O_3] + 2j_{H_2O_2}[H_2O_2] + 2j_{CH_2O \rightarrow H+HCO}[CH_2O] + 2j_{CHOCHO}[CHOCHO] + 2j_{CH_3OOH}[CH_3OOH] + 2j_{CH_3CHO}[CH_3CHO] + 2j_{CH_3C(O)CH_3}[CH_3C(O)CH_3] + 2j_{CH_3CH_2C(O)CH_3}[CH_3CH_2C(O)CH_2] \quad (5)$$

$$L(HO_x) = k_{NO_2+OH}[NO_2][OH] + \sum_i \alpha_{eff} k_{RO_{2,i}+NO}[RO_{2,i}^{\cdot}][NO] + 2k_{HO_2+HO_2}[HO_2][HO_2] + 2k_{RO_2+RO_2}[RO_2^{\cdot}][RO_2^{\cdot}] + 2k_{HO_2+RO_2}[HO_2][RO_2^{\cdot}] + net(PNs) \quad (6)$$

$$[RO_2^{\cdot}] = \frac{\sum_i k_{OH+VOC,i}[VOC_i][OH]}{(1-\alpha_{eff})k_{RO_2+NO}[NO] + k_{RO_2+HO_2}[HO_2]} \quad (7)$$

Here, k is the rate constant for compound, i, with the associated compound listed, $\alpha_{eff}$ is the effective branching ratio for R2a and R2b for the observations (Sect. 3.2), f is the fraction that $O^1D$ that reacts with water to form OH versus reacting with a third body molecule to form $O^3P$, β is the fraction the $R(O)O_2^{\cdot}$ that reacts with $NO_2$ versus NO, and j is the measured photolysis frequency (Table 2). In Eq. 5, only directly values directly measured on the DC-8 during KORUS-AQ are included. As discussed in Wang et al. (2022) and Sect. 4.3,, this is most likely an underestimations of $P(HO_x)$. Note, $R(O)O_2^{\cdot}$ is not included in Eq. 7 as (a) it is assumed the initial production of $R(O)O_2^{\cdot}$ is captured with the reaction of OH with VOC and (b) $R(O)O_2^{\cdot}$ accounts for a small

fraction of the total $RO_2$ (< 10%). Not including $R(O)O_2^{\cdot}$ in Eq. 7 may lead to a small underestimation of total $RO_2^{\cdot}$. Finally, $HO_2$ calculated from F0AM, rather than aircraft measurements (Crawford et al., 2021), is used in the equations to determine the $O_x$ and $HO_x$ budget (see Sect. S3, Figure S6).

## 3. Observational constraints on $NO_x$ organic oxidation chemistry

In the Sect. 3.1, the detailed observations from the DC-8 during KORUS-AQ provided measurements that allow us to test our understanding of $NO_x$ oxidation into total $NO_z$ ($NO_z$ = higher $NO_x$ oxides, including ΣPNs, ΣANs, $HNO_3$ and particulate nitrate, $pNO_3$), which is needed for the remainder of the analysis. Sect. 3.2 to 3.4 will focus on the organic $NO_z$ chemistry. This is due to the chemistry and dynamics impacting the total inorganic nitrate chemistry that has been discussed recently (Jordan et al., 2020; Travis et al., 2022).

### 3.1 $NO_x$ and its oxidation products

The average $NO_x$ mixing ratios observed by the NASA DC-8 in the SMA below 2 km after 11:00 local time is shown in Figure 1. As $NO_x$ is mainly emitted from anthropogenic activities, such as combustion emissions, in an urban environment, the largest $NO_x$ mixing ratios are observed between Olympic Park and the missed approach, as this area included downtown SMA. The missed approach included low level sampling at a military airport, which may have contributed to the $NO_x$ mixing ratios along with the activities throughout the SMA. As the DC-8 flies from the missed approach toward Taehwa Research Site, the $NO_x$ mixing ratios decreases. The combination of reduced emissions, chemical reactions, and dilution and mixing reduces the

262 $NO_x$ mixing ratios away from the city. An understanding of these processes is important for urban
263 $P(O_x)$.

264 On the DC-8, there were multiple measurements of various speciated and total family
265 contribution towards $NO_z$ (Table 2). The comparison of the speciated and measured $NO_z$ is
266 investigated in Figure 2 for observations over SMA. When only speciated PNs (GT) and ANs (CIT
267 + WAS) and gas-phase nitrate ($HNO_3$) are compared to the $NO_z$ ($NO_y$ (NCAR) – (NO (NCAR) +
268 $NO_2$ (TD-LIF)), only 46% of the $NO_z$ can be explained. This is not completely unexpected, as
269 multiple studies have indicated that the speciated ANs measurements are typically lower than the
270 total ANs measurements (Fisher et al., 2016; Perring et al., 2010). Further, $pNO_3$ has been found
271 to be important for total nitrate budget in the SMA (e.g., Travis et al., 2022). Chemiluminescence
272 measurements of gas-phase $NO_y$ have been found to efficiently measure $pNO_3$, depending on the
273 sensitivity to $pNO_3$ enhancements or exclusions (Bourgeois et al., 2022); thus, it is expected that
274 missing ANs and $pNO_3$ are necessary to close the $NO_z$ budget. Adding the measured $pNO_3$ to the
275 speciated PNs (GT) and ANs (CIT + WAS) and gas-phase nitric acid, 81% of $NO_z$ can be
276 explained. This barely overlaps the combined uncertainty of the measurements (~26%). Total PNs
277 and ANs, measured by TD-LIF, are needed to close of the total $NO_z$ budget.

278 The breakdown of the $NO_z$ budget over the SMA as the airmasses photochemically ages
279 (decreasing $NO_x$ contribution to total $NO_y$) is shown in Figure 2b. During KORUS-AQ, ~56% of
280 $NO_z$ was inorganic (gas- and particle-phase nitrate), ranging from 52% to 62%; the remaining $NO_z$
281 was organic (PNs and ANs). Approximately 74% of the total ANs were not speciated (range 73%
282 to 76%). Speciated PNs species, such as PAN (peroxy acetyl nitrate), account for a mean 51% of
283 the total PNs (range 47 to 59%), much lower than typically observed in prior studies (e.g.,
284 Wooldridge et al., 2010). In these prior studies, the speciated PN species (typically PAN + PPN

(peroxy propionyl nitrate)) accounted for 90 – 100% of the ΣPNs, except for some select cases attributed to poor inlet design (Wooldridge et al., 2010). PAN accounted for the majority of the speciated PNs, with the remaining speciated PNs (PPN + PBzN (peroxy benzoyl nitrate) + APAN (peroxy acryloyl nitrate)) accounting for ~1%. However, during KORUS-AQ, Lee et al. (2022) observed that PAN contributed only 60% of calculated total PNs in industrial plumes near the SMA. Thus, the VOC emissions in and near SMA potentially lead to PNs typically not directly measured; this is explored more in Sect. 3.4

As $NO_x$ decreases from ~30 ppbv to 4 ppbv, the contribution of organic $NO_z$ increases (Figure 2b). At about 4 ppbv, the contribution of organic $NO_z$ starts to decrease. Further, the contribution of the different organic $NO_z$ species changes. For example, from ~30 ppbv to 4 ppbv, the un-speciated ΣPNs contributes the majority of the organic $NO_z$ budget (~39%). Below ~4 ppbv, the contribution of un-speciated ΣPNs decreases and the PAN contribution increases. The change in contribution of PNs is due to changes in the PN precursors (e.g., combination short-lived precursors oxidizing to $CH_3C(O)O_2^{\cdot}$ and thermal decomposition of the higher PNs (higher PNs = ΣPNs – PAN)). On the other hand, the contribution of un-speciated ΣANs remains relatively constant with $NO_x$ (~6% of total $NO_z$). However, the type of ANs is most likely changing with $NO_x$ due to the lifetime of the ANs precursors and/or the lifetime of ANs. Less is known about the lifetime of ANs derived from anthropogenically emitted VOCs compared to those from biogenic VOCs (González-Sánchez et al., 2023; Picquet-Varrault et al., 2020; Zare et al., 2018). On average unknown ANs and PNs account for ~24% of the observed $NO_z$ on average. The differences in the binned mean value for each species is greater than the uncertainty associated with its measurements (maximum uncertainty 30%) and greater than the standard error of the mean, indicating that all the percent differences shown here are real.

### 3.2 Meteorological impact on $NO_x$ oxidation

As discussed in Sect. 2.1 and various prior studies, four different meteorological conditions impacted the observations during KORUS-AQ (Peterson et al., 2019). The impact of the meteorological conditions on $NO_x$ oxidation was investigated by plotting two metrics of $NO_x$ oxidation—$O_x$ versus ΣANs and ΣPNs versus formaldehyde (Figure 3). The implications of both plots are further discussed in Sect. 3.3 and 3.4, respectively. Briefly, $O_x$ versus ΣANs and ΣPNs versus formaldehyde are competitive products from the reaction of $RO_2^{\cdot}$ or $R(O)O_2^{\cdot}$ with $NO_x$ (R2a versus R2b or R8 versus R9). The different meteorological periods corresponded to differences in temperatures and amount of photolysis due to cloud cover (Peterson et al., 2019). Thus, these different periods may impact gas-phase chemistry and/or VOC emissions. However, as demonstrated in Figure 3, there are minimal systematic differences in the trends observed for the two $NO_x$ oxidation products as there is no systematic shift in the trends or scatter observed in Figure 3. This suggests that the data does not have to be separated by meteorological conditions.

### 3.3 Production of ANs to constrain R(VOC)

Observations of un-speciated ANs and PNs imply missing VOCs that impact $O_3$ chemistry. The relationship of ANs to $O_x$ can provide a method to investigate this source. This relationship provides an estimate of the effective branching ratio, α, for the observed VOC mix (Perring et al., 2013 and references therein). The value of this relationship stems from the reactions discussed above (R1 – R6) in that upon the oxidation of VOCs, some fraction of the time, $RO_2^{\cdot}$ reacts with NO to form an AN molecule and the remainder of the time the reaction goes to form $O_3$. This is expressed with the following equations:

$$P_{\Sigma ANs} = \sum \alpha_i \, k_{OH+VOCi}[\mathrm{OH}][\mathrm{VOC_i}] \quad (8)$$

$$P(\mathrm{O_x}) = \sum_i \gamma_i (1-\alpha_i) \, k_{OH+VOC_i}[\mathrm{OH}][\mathrm{VOC}_i] \quad (9)$$

Here, α is the effective branching ratio in the reaction of $RO_2^{\cdot}$ with NO to form ANs versus $RO^{\cdot}$ (R2), $k$ is the OH rate constant with VOC, i, and γ is the number of $O_3$ molecules formed per oxidation of VOC, i. The reactivity weighted γ is calculated for the observed and F0AM calculated species with Eq. 10, where γ for each compound is taken from MCM (Jenkin et al., 2015) and accounts for potential for difference number of $O_3$ molecules produced per channel per oxidation (e.g., xylene produces two $O_3$ molecules 60% of the time and one $O_3$ molecule 40% of the time). All the terms were defined for Eq. 8 – 9.

$$\gamma_{eff} = \frac{\sum_i \gamma_i k_{OH+VOC_i}[\mathrm{OH}][\mathrm{VOC_i}]}{\sum_i k_{OH+VOC_i}[\mathrm{OH}][\mathrm{VOC_i}]} \quad (10)$$

The reactivity weighted γ is found to be, on average, 1.53, which is lower than the value of 2 typically assumed in prior studies (e.g., Perring et al., 2013). This lower reactivity weighted γ is due to the role of CO (γ = 1) and $CH_2O$ (γ = 1) to the total reactivity. After the boundary layer height has stabilized (e.g., after 11:00 am LT used here) and is near enough (e.g., less than 1 day aging) to the VOC source to ignore deposition and entrainment, Eq. 8 and 9 can be combined to approximate the change in $O_x$ per molecule ΣAN formed:

$$\frac{\Delta O_x}{\Delta \Sigma ANs} \approx \frac{P_{O_x}}{P\Sigma ANs} \approx \frac{1.53(1-\alpha)}{\alpha} \quad (11)$$

For this equation to be valid, α needs to be relatively small (α << 1), which is true for VOCs, as maximum α for the conditions of KORUS-AQ is expected to be 0.35 (Orlando and Tyndall, 2012; Perring et al., 2013; Yeh and Ziemann, 2014). Note, though Eq. 11 can be used at short photochemical ages due to minimal impact from physical loss processes, chemical loss processes may impact the assumptions in Eq. 11 and are discussed in more detail below.

Over the SMA during KORUS-AQ, the slope between $O_x$ and ΣANs was observed to be 40.5±1.8 (Figure 3a), with an $R^2$ = 0.60. Using Eq. 11, this translates to an effective branching ratio ($\alpha_{eff}$), of 0.036. For other urban locations around the world, this slope has ranged from 13 – 47 (Farmer et al., 2011; Kenagy et al., 2020; Perring et al., 2010; Rosen et al., 2004), leading to an effective α between 0.04 and 0.15, assuming a γ of 2 instead of the calculated γ used here. Thus, the $\alpha_{eff}$ observed over SMA during KORUS-AQ is similar to other urban locations (Houston = 0.05 (Rosen et al., 2004) and South Korea = 0.05 (Kenagy et al., 2021)) but much lower than observed for Mexico City = 0.07 – 0.12 (Farmer et al., 2011; Perring et al., 2010) and Denver = 0.16 (Kenagy et al., 2020). This suggests that VOCs with low α dominate the total R(VOC) and production of ANs in SMA. The VOCs in SMA that dominate R(VOCs), including OVOCs, alkenes, and aromatics (Schroeder et al., 2020; Simpson et al., 2020), generally have lower α (Orlando and Tyndall, 2012; Perring et al., 2013 and references therein).

We use the observed VOCs (Table 2) and estimated secondary products from F0AM to calculate $\alpha_{eff}$ from this mixture to compare to the calculated $\alpha_{eff}$ of 0.036 derived from the slope of $O_x$ versus ΣANs in Figure 3a, as shown in Figure 4. To derive $\alpha_{eff}$, Eq. 12 was used, where all the terms are the same as Eq. 8 – 9.

$$\alpha_{eff} = \frac{\sum_i \alpha_i k_{OH+VOC_i}[\mathrm{OH}][\mathrm{VOC_i}]}{\sum_i \gamma_i k_{OH+VOC_i}[\mathrm{OH}][\mathrm{VOC_i}]} \quad (12)$$

The R(VOC) calculated from the observed VOCs and from the intermediates produced by the F0AM model, described in Sect. 2.2, are shown in Figure 4a, and the reactivity weighted α for the observations is shown in Figure 4b. As has been observed in other urban environments (e.g., Hansen et al., 2021; Whalley et al., 2016; Whalley et al., 2021; Yang et al., 2022), measured OVOCs contribute the most to the calculated R(VOC) for all $NO_x$ mixing ratios (32 – 48%). The unmeasured OVOCs (F0AM species) contributed 17 – 28% of the calculated reactivity. The F0AM

species reactivity ranged from 0.45 – 1.78 $s^{-1}$, which is a similar increase in total OH reactivity observed by Brune et al. (2022) over South Korea. At higher $NO_x$ mixing ratios, primary, more reactive VOCs (e.g., alkanes, alkenes, aromatics) contribute an important fraction (> 25%) of the R(VOC). As there are interferences in the total OH reactivity measurement at high $NO_x$ (Brune et al., 2022), we are unable to determine the extent to which the observed and modeled reactivity captures total OH reactivity in the SMA above a $NO_x$ value of approximately 4 ppbv. At lower $NO_x$ mixing ratios, ~33% of the R(VOC) is missing (calculated R(VOC), including F0AM species, ~3.0 $s^{-1}$ and measured R(VOC) from Penn State—see Table 2—is 4.5 $s^{-1}$).

Numerous other urban studies have observed unmeasured OH reactivity, which is assumed to be unmeasured R(VOC), as the inorganic OH reactivity is typically well covered by measurements. Here, we are defining unmeasured R(VOC) as the reactivity not represented by measurements on the DC-8 or by F0AM predicted species and reactivity. This unmeasured R(VOC) has ranged from ~3 $s^{-1}$ to ~10 $s^{-1}$ (e.g., Brune et al., 2022; Hansen et al., 2021; Kim et al., 2016; Ma et al., 2022; Tan et al., 2019; Whalley et al., 2016; Whalley et al., 2021). Over the SMA, the difference between measured and calculated R(VOC) was ~1.5 $s^{-1}$ at low $NO_x$ and unknown at high $NO_x$ mixing ratios. The lower difference may be related to the comparison occurring for observations at low $NO_x$, when the very reactive material has either reacted into compounds measured on the DC-8 (e.g., formaldehyde, acetaldehyde, etc.), diluted to low enough concentrations to be negligible for R(VOC), or undergone deposition or partitioning to the particle-phase.

At higher $NO_x$ mixing ratios, which is more representative of fresh emissions, these more reactive compounds typically not measured are expected to lead to a higher difference between the calculated and observed R(VOC). Prior studies with more comprehensive measurements found

these more reactive compounds and their secondary products contributed an important fraction towards the R(VOC) (e.g., Whalley et al., 2016). Thus, to determine if these unmeasured VOCs potentially contribute to the R(VOC), and thus $P(O_x)$, in SMA, another means to constrain their contributions is necessary. One potential means to constrain the total R(VOC) is by using the observed ΣANs and $O_x$ and assuming the observations are from the instantaneous production of both species (e.g., the assumption used for Figure 3a).

To estimate the unmeasured R(VOC), Eq. 13 is used without cancelling out terms and expanded into the measured and unmeasured R(VOC) and α:

$$\frac{\Delta O_x}{\Delta \sum ANs} = \frac{\gamma RVOC_m[\mathrm{OH}]+\gamma RVOC_u[\mathrm{OH}]-\gamma\alpha_m RVOC_m[\mathrm{OH}]-\gamma\alpha_u RVOC_u[\mathrm{OH}]}{\alpha_m RVOC_m[\mathrm{OH}]+\alpha_u RVOC_u[\mathrm{OH}]} \quad (13)$$

Here, $\frac{\Delta O_x}{\Delta \sum ANs}$ is the slope from Figure 3a, γ is the number of $O_3$ molecules formed per oxidation of VOC, which is 1.53 for this study, R(VOC) is the VOC reactivity, which is its OH oxidation rate constant and its concentration (k×[VOC]) in units $s^{-1}$, α is the branching ratio for R2 (Table 1), and *m* and *u* correspond to "measured" (measured VOCs on DC-8 along with secondary species predicted by F0AM) and "unmeasured" (unmeasured VOCs that are not represented by DC-8 observations and not predicted by F0AM) RVOC and α. The rate constants for the measured VOCs are listed in Table 1, the reactivity for F0AM is taken directly from F0AM, and α is either from MCM (Jenkin et al., 2015) or Perring et al. (2013) for observations or assumed to be 0.05 for F0AM secondary products. The equation is rearranged and solved for $RVOC_u$, using different values of $\alpha_u$ (e.g., 0.00 – 0.30, values typical α).

As discussed in Sect. S3 in the Supp. Information, there are numerous assumptions and potential sources of uncertainty in the simplified version of Eq. 13. A thorough analysis and discussion of these assumptions are discussed in Sect. S3. The potentially most important assumption is that chemical loss is negligible in solving Eq. 13. However, due to the expected

relatively short lifetime of ∑ANs, the chemical loss of both $O_x$ and ANs nearly cancel each other, leading to similar results in considering or neglecting these loss terms in Eq. 13. Further, as ∑ANs chemical loss has uncertainty, especially for ANs produced from anthropogenic VOC oxidation, the use of Eq. 13 reduces some of these uncertainties in comparison to Eq. S9. Thus, for the remainer of the paper, the values calculated from Eq. 13 will be used. Another limitation in this study is assuming a constant α and γ across all $NO_x$ mixing ratios to estimate the unmeasured R(VOC). At higher $NO_x$ mixing ratios, where the VOC mixing ratios would be highest due to being closer to emissions, it would be expected that both α and γ would change. However, the direction that these values would change is uncertain as both α and γ depend on the structure of the VOC, which is currently unknown.

For the range of missing α assumed, an α = 0.10 for the unmeasured R(VOC) provides the best agreement with the observed R(VOC) ("From PSU" is the Penn State OH Reactivity with inorganic reactivity subtracted out) for all observations where $NO_x$ < 4 ppbv. Further, it is found that α ranging from 0.075 – 0.125 encompasses the associated uncertainty with the observed R(VOC) (±0.64 $s^{-1}$ (Brune et al., 2019)). This leads to an average unmeasured R(VOC) of $1.7^{+1.1}_{-0.4}$.

The associated total missing R(VOC) for the assumed α of 0.10 ranges from 1.5 to 2.8 $s^{-1}$ (Figure 4a upper panel). Assuming typical rate constants for emitted VOCs, assuming it is comparable to semi- and intermediate-VOCs, and their associated secondary products (~$1 – 4\times10^{-11}$ $cm^3$ $molec.^{-1}$ $s^{-1}$ (Ma et al., 2017; Zhao et al., 2014)), the total missing reactivity would be equivalent to ~1 – 8 ppbv. Zhao et al. (2014) observed ~12 μg $m^{-3}$ of semi- and intermediate-VOCs near Los Angeles, CA, during the CalNex study. Depending on the molecular weight assumed, this translates to ~1 to 2 ppbv. Nault et al. (2018) found that ~5 – 8 ppbv of VOCs were needed to explain the observed secondary organic aerosol production over the SMA, depending on the

molecular weight assumed for the VOC. Further, Kenagy et al. (2021) also found that known chemistry could only account for ~33% of the observed ANs and missing sources of lower volatility VOCs to produce anthropogenically-derived ANs were necessary. Finally, Whalley et al. (2016) found that addition of unassigned VOCs and their associated oxidation products led to a reactivity of ~1.6 $s^{-1}$, leading to ~1 – 6 ppbv missing R(VOC). Thus, the reactivity and equivalent mixing ratios estimated here appear plausible and warrant future measurements to understand this unmeasured reactivity sources.

One important aspect of this unmeasured R(VOC) is that it should not be considered one or a couple of VOCs emitted and contributing 1 – 8 ppbv of VOC in the atmosphere. Instead, it will be the emitted VOCs and its oxidation products summed together to form the 1 – 8 ppbv of unmeasured VOCs in the atmosphere.

One possible group of missing VOCs are long-chain aldehydes from cooking and vegetative emissions, including nonanal (Hurst Bowman et al., 2003; Rao et al., 2010; Sai et al., 2012; Schauer et al., 2002). Kim et al. (2018) observed cooking organic aerosols at a ground site in SMA, indicating that there should be associated gas-phase emissions from cooking. Higher carbon aldehydes (or cycloalkanes) have been recently suggested to be a potential interference compound with isoprene measurements on a PTR-MS (Coggon et al., 2024; Wargocki et al., 2023). Comparisons of isoprene measured by the PTR-MS and WAS during KORUS-AQ (Figure S7) shows at increasing $NO_x$ mixing ratios (closer to emission sources), the difference between the PTR-MS and WAS isoprene mixing ratios increases. This suggests that there are potential unmeasured OVOCs and/or other $C_5H_8$ alkenes at high $NO_x$ ratios that cannot be easily determined by the difference between the PTR-MS and WAS. Continuing to use nonanal as a surrogate for this unmeasured OVOC, nonanal has a rate constant consistent with the values used above for the

468 missing R(VOC) ($3.6\times10^{-11}$ $cm^3$ $molec.^{-1}$ $s^{-1}$ (Hurst Bowman et al., 2003)). Further, nonanal has
469 an estimated high α of ~0.2 (Hurst Bowman et al., 2003). As typical nonanal mixing ratios have
470 been observed or estimated to be < 500 pptv, this suggests that nonanal or similar OVOCs may
471 contribute to some of the missing reactivity (< 0.45 $s^{-1}$). Finally, nonanal and other long-chain
472 aldehydes may be an important higher PNs precursor (see Sect. 3.4 for more discussion about un-
473 speciated higher PNs).

474 OVOC emissions from multiple sources, including solvent evaporation and other non-
475 transportation emissions, are generally considered to be an important fraction of R(VOC) for urban
476 emissions but may not be measurable by PTR or GC, such as glycols (de Gouw et al., 2018;
477 Gkatzelis et al., 2021; McDonald et al., 2018; Ma et al., 2022; Simpson et al., 2020; Wang et al.,
478 2022; Yang et al., 2022). However, the α for OVOC is potentially smaller than alkanes, though it
479 is highly unconstrained (Orlando and Tyndall, 2012). Note, higher OVOCs have been understudied
480 and thus may have higher α (e.g., nonanal). Thus, if the missing reactivity is mainly OVOCs and
481 it is assumed their α is low, compounds with α > 0.15 will be needed for the budget closure shown
482 here. Likely compounds with high α include alkanes, cycloalkenes/alkenes, and aromatics, though
483 the latter is also highly uncertain. Alkanes have typically been a small source for the R(VOC) in
484 urban environments (e.g., McDonald et al., 2018; Simpson et al., 2020; Whalley et al., 2016).
485 Though aromatics contribute a significant fraction of R(VOC) in different Asian urban
486 environments (Brune et al., 2022; Schroeder et al., 2020; Simpson et al., 2020; Whalley et al.,
487 2021), the majority of the aromatic R(VOC) is considered to be measured by WAS over SMA
488 during KORUS-AQ (e.g., measured aromatics account for ~81% of aromatic reactivity in
489 McDonald et al. (2018) and 98% of aromatic reactivity in Whalley et al. (2016), where both studies
490 had more complete VOC measurements). Finally, the cycloalkenes/alkenes originate from

numerous anthropogenic sources (e.g., McDonald et al., 2018; Simpson et al., 2020). One subclass of cycloalkenes includes monoterpenes. Similar to the comparison of isoprene between PTR-MS and WAS, the difference in monoterpenes between these two measurements increases with increasing $NO_x$ (Figure S8). As the interfering compound(s) measured by the PTR-MS and whether they are oxygenated or not is not known, only the WAS monoterpenes are used in this analysis of calculating R(VOC). Assuming the limonene rate constant, the difference between the PTR-MS and WAS monoterpenes raises the terpene reactivity by 0.05 – 0.30 $s^{-1}$. Though this does not include any associated photochemical products from the oxidation of monoterpenes and can improve the closure, it does not explain the total missing reactivity (1.4 – 2.1 $s^{-1}$). Thus, the missing R(VOC) is most likely a combination of OVOCs and cycloalkenes/alkenes.

### 3.4 Sources of PNs over SMA

As shown in Figure 2, ΣPNs account for a larger fraction of the total $NO_z$ budget than ΣANs. ΣPNs are known to be a temporary sink of $NO_x$ and radicals ($R(O)O_2^{\cdot}$) due to their short thermal lifetime (~1 hr). Thus, the $NO_x$ emitted in SMA is being transported regionally, impacting the $P(O_x)$.

In Figure 3b, ΣPNs shows some correlation with formaldehyde. Both are secondary products from the photooxidation of VOCs and have short lifetimes, leading to the correlation. However, above 4 ppbv formaldehyde, the correlation shifts as ΣPNs increases more rapidly than formaldehyde. As shown in Figure S9, this change in the relationship between ΣPNs versus formaldehyde is due to changes in the competition in the reaction of the acyl peroxy radical ($R(O)O_2^{\cdot}$) between $NO_2$ and NO. At low NO-to-$NO_2$ ratios, R8 is more favorable, as the $R(O)O_2^{\cdot}$ is more likely to react with $NO_2$ compared with NO, leading to more efficient production over

formaldehyde. As the NO-to-$NO_2$ ratios increase (NO becomes comparable to $NO_2$, leading to more equal probability in $R(O)O_2^{\cdot}$ reacting to NO and $NO_2$, leading to production of alkoxy radicals that can form formaldehyde), R9 becomes more dominant, leading to less production of PNs.

To further explore the sources of both PAN and the higher ΣPNs, the F0AM model (Wolfe et al., 2016) was used to predict both unmeasured ΣPNs, constrained by the observed VOCs precursors, PAN, and PPN (Table 2) and budget of all ΣPNs, where PAN and PPN were not constrained. F0AM shows minimal bias in the predicted formaldehyde, $NO_2$, and OH (Figure S10) when PAN and PPN were constrained. As discussed in Sect. 3.3, though, there is missing R(VOC) of $1.7^{+1.1}_{-0.4}$s$^{-1}$. A sensitivity analysis in adding this missing reactivity to F0AM on predicted OH and formaldehyde was conducted (Sect. S4 and Figure S11 – S12). Both OH and formaldehyde are found to be buffered with the addition of this low amount of R(VOC). Thus, though there is good agreement in these intermediate products between observation and F0AM, this analysis for the sources of PAN and higher ΣPNs is expected to be a lower limit. This missing R(VOC) is further observed in the F0AM-predicted higher PNs (ΣPNs without PAN, or ΣPNs-PAN for short) versus formaldehyde, as a general underestimation in the total higher PNs compared to observations is observed (Figure 5a). (Schroeder et al., 2020)

The classes of compounds producing higher PNs in F0AM are shown in Figure 5b. The classes of compounds were selected from the parent VOC which was oxidized into the higher PN (Table S2). Individual PNs with high contributions and/or are typically measured (PPN, PBzN, and MPAN (methacryloyl peroxy nitrate)) or are a large fraction of PNs but have yet to be measured in ambient conditions (PHAN) are shown without any connection to the parent VOC. Further, both PHAN and PPN have numerous precursors while many of the other higher PNs

modeled by F0AM are generally associated with one precursor. At high $NO_x$ mixing ratios, the more reactive VOCs (aromatics, terpenes) contribute a large fraction of the higher PNs (>35% for $NO_x$ > 4 ppbv). As the air moves away from SMA (lower $NO_x$ mixing ratios), contributions of higher PNs from longer-lived compounds (e.g., alkanes) and later generation oxidation products start dominating.

An interesting trend is observed for PPN and PHAN. Both peroxy acyl radicals for PPN and PHAN ($C_2H_5C(O)O_2^{\cdot}$ and $CH_2(OH)C(O)O_2^{\cdot}$, respectively) are products from photooxidation of many VOCs, including aromatics, alkanes, and methyl ethyl ketone (MEK). However, the fractional contribution of PPN to higher PNs remains constant with decreasing $NO_x$ while the fractional contribution of PHAN increases with decreasing $NO_x$ (Figure 5b). This stems from the sources of $C_2H_5C(O)O_2^{\cdot}$ versus $CH_2(OH)C(O)O_2^{\cdot}$. The MCM mechanism, which is used for F0AM, produces $C_2H_5C(O)O_2^{\cdot}$ from the photooxidation from both short- and long-lived species (isoprene, C8-aromatics, toluene, ethanol, MEK, propane, and C4-alkanes) while $CH_2(OH)C(O)O_2^{\cdot}$ is produced from the photooxidation of isoprene and ethene. For $CH_2(OH)C(O)O_2^{\cdot}$, the production is through minor channels in the photooxidation of isoprene (~3% yield directly from isoprene and ~20% as a secondary product (Galloway et al., 2011)). Ethene is relatively long-lived, with a lifetime ~7 hrs (OH = $5\times10^6$ molec. $cm^{-3}$) leading to the delay in the production of PHAN. Note, PHAN formation in MCM/F0AM may be overestimated, as Butkovskaya et al. (2006) found that the radical formed from the photooxidation of glycolaldehyde decomposes to form formaldehyde and $CO_2$, potentially competing with the pathway to form PHAN. Other studies also found that PNs were not observed by photooxidation of glycoaldehyde (Magneron et al., 2005).

559 The results here in general indicate more speciated measurements of higher PNs are
560 needed. However, as highlighted in Figure 5, improved detection or measurements of PBzN,
561 PHAN, and MPAN would allow for furthering our knowledge in PNs chemistry in urban
562 environments and their role in controlling $O_x$ production.

563 A qualitative investigation of the precursors of PAN predicted by F0AM are shown in
564 Figure 5c. This provides a basis for further investigation of the sources over the SMA region for
565 PAN as (a) F0AM over-predicts PAN, as noted above, (b) ethanol is currently estimated, similar
566 to Schroeder et al. (2020), and (c) R(VOC) in F0AM is low due to missing precursors. Like the
567 higher PNs, highly reactive R(VOC) contributes a large portion of the PAN budget at high $NO_x$.
568 The short-lived compounds contribute ~80% of PAN over SMA at the highest $NO_x$ mixing ratios.
569 At lower $NO_x$ mixing ratios, moving away from SMA, longer-lived compounds, such as ethanol,
570 contribute the most towards PAN production (~70%).

571 One of the interesting contributions not typically observed for PAN is MEK, which also
572 contributes to PPN and PHAN. In prior studies, MEK mixing ratios were typically 0.5 to 2.0 ppbv
573 (Bon et al., 2011; de Gouw et al., 2018; Liu et al., 2015). Over the SMA, 1.5 ppbv of MEK was
574 observed on average with values as high as 8.3 ppbv. Due to the long lifetime of MEK (~30 hrs
575 for the average photolysis rate measured and OH = $5\times10^6$ molec. $cm^{-3}$), the high mixing ratios of
576 MEK are most likely due to direct emissions (e.g., de Gouw et al., 2005; Liu et al., 2015). Thus,
577 there are potentially large sources of MEK in SMA that need to be considered in properly
578 representing PAN chemistry.

579 Another potentially important compound for PAN production is ethanol. However, this
580 compound was not measured during KORUS-AQ; instead, it was estimated based on previous
581 ground-based observations, similar to Schroeder et al. (2020). Ethanol is considered to mainly

come from both vehicle emissions (e.g., Millet et al., 2012) and non-transportation emissions, including cleaning agents and solvents (e.g., McDonald et al., 2018). As ethanol use is predicted to increase in the future (e.g., de Gouw et al., 2012) and cleaning agents and other volatile chemical products appear to scale with population (Gkatzelis et al., 2021), ethanol and MEK may continue contributing towards the PAN budget in the SMA in the future.

As a note, two other compounds potentially important for PAN production that were not measured on the DC-8 during KORUS-AQ include methylglyoxal and biacetyl (LaFranchi et al., 2009). In a forested environment that was partially impacted by urban outflow, these two components contributed on average 25% of the PAN budget (LaFranchi et al., 2009). In urban environments, methylglyoxal is believed to mainly originate from aromatic oxidation (Ling et al., 2020); whereas, biacetyl is believed to come from anthropogenic emissions (Xu et al., 2023). Further, as discussed in Sect. 4.3, these two compounds may potentially be important missing $HO_x$ sources, as well. Thus, measurements of these two compounds along with ethanol is necessary to better understand PAN chemistry.

## 4. Observational constraints of the $HO_x$ and $O_x$ budget over SMA

As highlighted in Figure S1, the three factors impacting instantaneous $P(O_x)$ are R(VOC), $P(HO_x)$, and $NO_x$ loss processes. In Sect. 3, the $NO_x$ loss processes were investigated and provided a constraint for R(VOC) to improve the investigation of $P(O_x)$. With R(VOC) constrained, the $RO_2^{\cdot}$ concentration can be estimated, providing a means to calculate the net $P(O_x)$ and to investigate the major reactions leading to $O_x$ loss and total $HO_x$ ($OH + HO_2 + RO_2^{\cdot} + R(O)O_2^{\cdot}$) loss. With the latter, this allows for an investigation of the major $P(HO_x)$ reactions, assuming $L(HO_x)$ equals $P(HO_x)$ (see Eq. 1 – 7 in Sect. 2.3).

### 4.1 Net $O_x$ production and sources of $O_x$ loss

Using the total R(VOC) from Sect. 3.3 (Figure 4a), the net $P(O_x)$ (Eq. 1 – 2) over SMA during KORUS-AQ has been determined (Figure 6a). The net $P(O_x)$ peaked at 9.3 ppbv $hr^{-1}$ at ~8 ppbv $NO_x$. If only the measured and estimated R(VOC) from F0AM secondary products is used to calculate net $P(O_x)$, the value decreases to 7.6 ppbv $hr^{-1}$, but at the same $NO_x$ mixing ratio. This value is similar to values observed in other urban locations around the world (~2 – 20 ppbv $hr^{-1}$), showing that many urban areas are still impacted by high $P(O_x)$ values (Brune et al., 2022; Griffith et al., 2016; Ma et al., 2022; Ren et al., 2013; Schroeder et al., 2020; Whalley et al., 2016, 2018).

The $NO_x$ distribution over SMA (Figure 1) shows a large area (~127.53°E to 127.18°E, or ~39 km), which corresponds to the $NO_x$ mixing ratio that results in maximum $P(O_x)$, as shown in Figure 6a. Thus, a large portion of the SMA will have high instantaneous $P(O_x)$ of ~9 ppbv $hr^{-1}$. As the median wind speed over SMA during KORUS-AQ was ~5 m $s^{-1}$, an air parcel would remain at the highest $P(O_x)$ for ~2 hrs, leading to ~18 ppbv $O_3$ being produced (not including dilution). This agrees with the ~20 ppbv increase in $O_3$ observed over the Taehwa Research Forest supersite between midday and afternoon overpasses by the DC-8 during KORUS-AQ (Crawford et al., 2021). Thus, though there is a substantial $O_3$ background observed over SMA (Colombi et al., 2023; Crawford et al., 2021), a large contribution of the $O_3$ is due to photochemical production.

The major reactions leading to $O_x$ loss ($L(O_x)$) are shown in Figure 6b. The two major reactions that lead to $O_x$ loss are net R8 (light and dark red), or the net production of PNs (which includes losses), and R11, reaction of $NO_2$ with OH (blue) (see Table 1). Note, as discussed in Sect. 2.2, for the budget analysis conducted here, PAN and PPN were constrained to observations. At high $NO_x$ (near emissions, ~30 ppbv), R11 ($NO_2$ + OH) dominates the $L(O_x)$ budget (> 60%),

with net R8 (net PAN, dark red, and higher PNs, light red) contributing ~25%, and R12 – 14 accounting for the remaining 15% of $O_x$ loss. As $NO_x$ mixing ratios decrease (moving away from emissions), the net R8 reaction, producing both PAN and higher PNs, starts contributing to larger total $L(O_x)$, ranging from 30 – 40%. Furthermore, the net R8 reaction contribution towards $L(O_x)$ remains relatively constants with $NO_x$ mixing ratios as the contribution from R11 ($OH + NO_2$) decreases. At $NO_x$ mixing ratios < 3 ppbv is when non-$NO_x$ reactions (R12 – 14) contribute greater than 30% of the $L(O_x)$ budget. Thus, proper representation of PAN and higher PNs, both in precursors and speciation, is important in properly understanding the $O_x$ budget in SMA.

### 4.2 $HO_x$ loss over the SMA

Similar to $L(O_x)$, the major reactions leading to $L(HO_x)$ over the SMA during KORUS-AQ were the reactions of $NO_x$ with $HO_x$, specifically $NO_2$ with OH (R11) and net PAN (dark red) and higher PNs (light red) production (R8) (Figure 6c). Reaction R11 is most important for $NO_x$ mixing ratios greater than 15 ppbv (50 – 65%). Between 5 and 15 ppbv, R11 is comparable to the net PN production (R8), where R11 comprises 35 – 50% of $L(HO_x)$ while net R8 (sum of higher $\sum$PNs and PAN) comprises 30 – 40% of $L(HO_x)$. At lower $NO_x$ mixing ratios, R11 is always smaller for $L(HO_x)$ than net R8, where R11 is about a factor of 2 lower than net R8. Production of $\Sigma$ANs played a minor role due to the low $\alpha_{eff}$.

The self-reaction of $HO_x$ species (R15 – R16) contributes minimally to $L(HO_x)$ (less than 10%) for $NO_x$ mixing ratios greater than 8 ppbv. At lower $NO_x$ mixing ratios, R16 starts dominating $L(HO_x)$ budget, increasing from 8% at 8 ppbv to 50% of $L(HO_x)$ at $NO_x$ mixing ratios less than 2 ppbv. Reaction R15 remains relatively small for the $L(HO_x)$ budget, only reaching 7% of the $L(HO_x)$ budget at $NO_x$ mixing ratios less than 2 ppbv.

### 4.3 Sources of $HO_x$ over SMA

The analysis conducted leads to the ability to constrain $HO_x$ losses over the SMA during KORUS-AQ. This is important as not all typical $HO_x$ sources were measured on the DC-8 during the project (e.g., nitrous acid, or HONO), and $HO_x$ production rates directly impacts $P(O_x)$ (Figure S1). Prior studies (e.g., Griffith et al., 2016; Tan et al., 2019; Whalley et al., 2018) have demonstrated that in urban environments, sources of $HO_x$ include photolysis of $O_3$ and subsequent reaction with water vapor, formaldehyde photolysis, and HONO photolysis. Furthermore, recent studies have highlighted the potential importance of typically non-measured OVOCs in their contribution to $P(HO_x)$ and subsequent $P(O_x)$ in an urban environment (Wang et al., 2022). To constrain the $P(HO_x)$ over SMA during KORUS-AQ, the $P(HO_x)$ was assumed to be equal to the observationally constrained $L(HO_x)$. Then, $P(HO_x)$ was calculated for the measurements on the DC-8, including photolysis of $O_3$, formaldehyde, $H_2O_2$, and other measured OVOCs (Table 2).

Comparing the calculated $P(HO_x)$ and $L(HO_x)$, ~1.5 ppbv $hr^{-1}$ $P(HO_x)$ (range 1.3 – 1.8 ppbv $hr^{-1}$) is not accounted for, leading to ~45% of the necessary $L(HO_x)$ to maintain steady-state (Figure 7). For the calculated $P(HO_x)$ budget, $O_3$ and formaldehyde photolysis contributed ~50% and 40% of the budget, respectively, with the remainder coming from photolysis of $H_2O_2$ and other measured OVOCs. Accounting for the unobserved $P(HO_x)$, $O_3$ and formaldehyde photolysis contributed ~25% and ~20%, respectively.

Potential missing sources of $P(HO_x)$ are briefly speculated here. First, one potential source is the photolysis of methylglyoxal. Using the F0AM predicted methylglyoxal, as it was not measured on the DC-8, methylglyoxal would contribute ~0.24 ppbv $hr^{-1}$ $P(HO_x)$, or ~16% of the unobserved $P(HO_x)$. Another OVOC not measured on the DC-8 and expected to originate from

anthropogenic emissions and not from chemistry is 2,3-butanedione, or biacetyl (de Gouw et al., 2018; Grosjean et al., 2002; Schauer et al., 2002; Xu et al., 2023; Zhou et al., 2020). Prior studies observed 20 – 400 pptv of biacetyl (de Gouw et al., 2018; Xu et al., 2023), correspond to 0.04 – 0.74 ppbv $hr^{-1}$, or 3 – 49% of the unobserved $P(HO_x)$. Thus, between these two OVOCs, 19 – 66% of the unobserved $P(HO_x)$ could be explained. Other unmeasured OVOCs could potentially contribute to the observed $P(HO_x)$ (e.g., Wang et al., 2022); however, there is less constraints both on the speciation and photolysis rates for these OVOCs (e.g., Mellouki et al., 2015). Finally, HONO could contribute to this observed $P(HO_x)$. Up to 700 pptv of HONO was observed in SMA during KORUS-AQ (Gil et al., 2021), though, this would quickly photolyze to the altitudes the DC-8 flew over SMA (Tuite et al., 2021). Even at 50 – 100 pptv HONO, photolysis of HONO would lead to 0.2 – 0.4 ppbv $hr^{-1}$ $P(HO_x)$, or 13 – 27% of the unobserved $P(HO_x)$. Thus, between methylglyoxal, biacetyl, and HONO, between 32 – 92% of the unobserved $P(HO_x)$ could be accounted for. This analysis highlights the importance of measuring these $HO_x$ sources to better understand and constrain $O_x$ chemistry in SMA and other urban environments.

A comparison of $HO_x$ sources from F0AM is shown in Figure S14. As it has more complete OVOCs than the observations, the contributions are different than shown in Figure 7. Both observations and F0AM agree that photolysis of $O_3$ and subsequent reaction with water (R12) and photolysis of formaldehyde are the two largest sources of $HO_x$. F0AM also shows that methylglyoxal is an important source of $HO_x$, which is not shown in Figure 7 as methylglyoxal was not measured. However, the total F0AM $P(HO_x)$ was ~2.4 ppbv $hr^{-1}$, which was lower than the observationally constrained value. This further supports either potential unmeasured OVOCs coming from both emissions and chemistry and/or uncertainty in the photolysis rate constants for these OVOCs (e.g., Wang et al., 2022).

One note about this analysis is that particulate matter collected onto the downwelling CAFS optics during KORUS-AQ (see Sect. S5, Table S3, and Figure S13). Corrections of up to 20% were determined, and the associated uncertainties were also increased by 20% due to the corrections. Thus, the exact amount of unmeasured $P(HO_x)$ is potentially smaller than discussed.

## 5. Conclusions and Implications

In the Seoul Metropolitan Area (SMA), the ozone ($O_3$) mixing ratio often exceeds current standards and is increasing. Many processes can impact the $O_3$ mixing ratios and exceedances. Here, the processes that impact instantaneous $O_3$ production ($P(O_x)$, where $O_x$ is $O_3$ + $NO_2$ to account for possible $O_3$ titration) were investigated for observations collected on the NASA DC-8 during the 2016 NIER/NASA Korea United-States Air Quality (KORUS-AQ) study. The observations indicate missing oxidized $NO_x$ products ($NO_z$) that include both the short-lived peroxy nitrates (ΣPNs) and alkyl and multi-functional nitrates (ΣANs). ΣPNs contributed the most for the organic $NO_z$ species. Only ~50% of the ΣPNs were speciated over SMA, which is atypical as prior studies typically show closure between the speciated and total PN measurements.

The un-speciated ΣPNs and ΣANs were used to constrain the missing volatile organic compound (VOC) reactivity (R(VOC)), as R(VOC) is important in constraining the instantaneous $P(O_3)$. The missing R(VOC) was found to be 1.4 to 2.1 $s^{-1}$. The F0AM box model further supports the role of unmeasured ΣPNs as an important temporary $NO_x$ and radical sink over SMA. F0AM predicts ~50% of the higher ΣPNs (higher ΣPNs = ΣPNs – PAN), indicating missing R(VOCs) may explain the other 50%. Constraints from both the ΣPNs and ΣANs suggest that this missing R(VOC) would include oxygenated VOCs (OVOCs), including aldehydes such as octanal and nonanal from cooking, and alkenes from anthropogenic emissions.

With the constraints on the R(VOC), the net instantaneous $P(O_x)$ was determined for SMA. It was found to peak at ~10 ppbv $hr^{-1}$ at ~8 ppbv $NO_x$. A large fraction of the SMA area was, on average, at this mixing ratio of $NO_x$, indicating high local $P(O_x)$. This supports the increase of ~20 ppbv of $O_3$ observed in a downwind site (Taehwa Research Forest supersite) from midday to afternoon during KORUS-AQ.

With the comprehensive measurements on-board the DC-8, the F0AM model results, and the observationally constrained R(VOC), a budget analysis on the sinks of $O_3$ ($L(O_x)$) and $HO_x$ ($L(HO_x)$, where $HO_x = OH + HO_2 + RO_2^{\cdot} + R(O)O_2^{\cdot}$) was performed. Due to the high R(VOC), type of VOC, and the $NO_2$-to-NO ratio, net ΣPNs production is surprisingly a large and important sink of $O_x$ and $HO_x$ over SMA (~25 – 40% and 15 – 40% for $L(O_x)$ and $L(HO_x)$, respectively), with production of $HNO_3$ and radical self-reactions accounting for the other $L(O_x)$ and $L(HO_x)$ losses. Net ΣPNs production as an important $L(O_x)$ and $L(HO_x)$ term is significant, as ΣPNs is a temporary reservoir of both $NO_2$ and $R(O)O_2^{\cdot}$ but has not traditionally been included in these calculations. Downwind locations separated from the local $NO_x$ and VOC emissions of the SMA will experience increased $P(O_x)$ due to the release of $NO_2$ and $R(O)O_2^{\cdot}$. With the constraint of $L(HO_x)$, $P(HO_x)$ was investigated, assuming steady-state, and unmeasured HONO plus unmeasured OVOCs were found to be necessary to explain the missing $HO_x$ sources. Both sources of $HO_x$ are either missing or highly uncertain in chemical transport models.

Though the high regional background and foreign sources of $O_3$ and its precursors elevate the $O_3$ levels in SMA and potentially already causes the SMA to be in exceedance for $O_3$ concentrations, this study highlights the importance local, in-situ $P(O_x)$ to the SMA area, which can further exacerbate the $O_3$ concentrations for SMA and the surrounding region. The results support the observations of increasing $O_3$ with decreasing $NO_x$ that has been observed for SMA in

743 prior studies. Further, the study highlights the important role of unmeasured VOCs and OVOCs
744 and the necessity to understand their sources and role in $NO_x$ and $O_3$ chemistry. Further, the study
745 demonstrates the interplay of direct emissions or secondary production of PN precursors and its
746 role in net $P(O_x)$. Attempts at specifically reducing the sources of PN may adversely impact net
747 $P(O_x)$, as lower net PN chemistry may increase $O_3$ due to more $NO_2$ being available.

## Competing Interests

At least one of the (co-)authors is a member of the editorial board of Atmospheric Chemistry and Physics.


## Acknowledgements

The authors acknowledge Michelle Kim, Alex Teng, John Crounse, and Paul O. Wennberg for their measurements with CIT-CIMS ($HNO_3$, multifunctional alkyl nitrates, and OVOCs), William H. Brune for his measurements with ATHOS (OH, OH reactivity), Alan Fried for his measurements with CAMS ($CH_2O$ and $C_2H_6$), Paul Romer-Present for his contribution to collecting data with TD-LIF, Sally Pusede for her contributions to collecting data with DACOM and DLH, and Andrew J. Weinheimer for his measurements of NO, $O_3$, and $NO_y$. The PTR-MS instrument team (P. Eichler, L. Kaser, T. Mikoviny, M. Müller) are acknowledged for their support.

## Funding

BAN and KRT acknowledge NASA grant 80NSSC22K0283. LGH and YL acknowledge NASA grant NNX15AT90G for the PAN measurements. SRH and KU were supported by NASA grant NNX15AT99G for photolysis measurements. AW acknowledges support by the Austrian Federal Ministry for Transport, Innovation, and Technology (bmvit-FFG-ASA) for the PTR-MAS measurements. PCJ and JLJ were supported by NASA 80NSSC21K1451 and 80NSSC23K0828.


## Data Availability

Version R6 1-min merged data used in this analysis available at DOI:10.5067/Suborbital/KORUSAQ/DATA01. The F0AM setup file, input file, and output files are all available at https://doi.org/10.5281/zenodo.10723227.

**Author Contribution**

BAN, KRT, and JHC designed the experiment and wrote the paper. BAN and KRT analyzed the data. KRT ran the F0AM model and KRT and BAN analyzed the model output. BAN, DRB, PCJ, RCC, JPD, GSD, SRH, LGH, JLJ, K-EK, YL, IJS, KU, and AW collected and QA/QC the data during KORUS-AQ. All authors contributed to the writing and editing of the paper.

## References


Archibald, A. T., Neu, J. L., Elshorbany, Y. F., Cooper, O. R., Young, P. J., Akiyoshi, H., Cox, R. A., Coyle, M., Derwent, R. G., Deushi, M., Finco, A., Frost, G. J., Galbally, I. E., Gerosa, G., Granier, C., Griffiths, P. T., Hossaini, R., Hu, L., Jöckel, P., Josse, B., Lin, M. Y., Mertens, M., Morgenstern, O., Naja, M., Naik, V., Oltmans, S., Plummer, D. A., Revell, L. E., Saiz-Lopez, A., Saxena, P., Shin, Y. M., Shahid, I., Shallcross, D., Tilmes, S., Trickl, T., Wallington, T. J., Wang, T., Worden, H. M., and Zeng, G.: Tropospheric ozone assessment report: A critical review of changes in the tropospheric ozone burden and budget from 1850 to 2100, https://doi.org/10.1525/elementa.2020.034, 2020.

Atkinson, R.: Kinetics of the gas-phase reactions of OH radicals with alkanes and cycloalkanes, Atmos Chem Phys, 3, 2233–2307, https://doi.org/10.5194/acp-3-2233-2003, 2003.

Atkinson, R. and Arey, J.: Atmospheric Degradation of Volatile Organic Compounds, Chem Rev, 103, 4605–4638, https://doi.org/10.1021/CR0206420, 2003.

Atkinson, R., Baulch, D. L., Cox, R. A., Crowley, J. N., Hampson, R. F., Hynes, R. G., Jenkin, M. E., Rossi, M. J., and Troe, J.: Evaluated kinetic and photochemical data for atmospheric chemistry: Volume II - gas phase reactions of organic species, Atmos Chem Phys, 6, 3625–4055, https://doi.org/10.5194/acp-6-3625-2006, 2006.

Bohn, B. and Zetzsch, C.: Kinetics and mechanism of the reaction of OH with the trimethylbenzenes – experimental evidence for the formation of adduct isomers, Physical Chemistry Chemical Physics, 14, 13933, https://doi.org/10.1039/c2cp42434g, 2012.

Bon, D. M., Ulbrich, I. M., De Gouw, J. a., Warneke, C., Kuster, W. C., Alexander, M. L., Baker, a., Beyersdorf, a. J., Blake, D., Fall, R., Jimenez, J. L., Herndon, S. C., Huey, L. G., Knighton, W. B., Ortega, J., Springston, S., and Vargas, O.: Measurements of volatile organic compounds at a suburban ground site (T1) in Mexico City during the MILAGRO 2006 campaign: measurement comparison, emission ratios, and source attribution, Atmos Chem Phys, 11, 2399–2421, https://doi.org/10.5194/acp-11-2399-2011, 2011.

Bourgeois, I., Peischl, J., Neuman, J. A., Brown, S. S., Allen, H. M., Campuzano-jost, P., Coggon, M. M., Digangi, J. P., Diskin, G. S., Gilman, J. B., Gkatzelis, G. I., Guo, H., Halliday, H. A., Hanisco, T. F., Holmes, C. D., Nault, B. A., Nowak, J. B., Pagonis, D., Rickly, P. S., Robinson, M. A., Veres, P. R., Warneke, C., Wennberg, P. O., Washenfelder, R. A., and Wiggins, E. B.: Comparison of airborne measurements of NO, $NO_2$, HONO, $NO_y$, and CO during FIREX-AQ, Atmos Meas Tech, 15, 4901–4930, https://doi.org/10.5194/amt-15-4901-2022, 2022.

Brune, W. H., Miller, D. O., Thames, A. B., Allen, H. M., Apel, E. C., Blake, D. R., and Bui, T. P.: Exploring Oxidation in the Remote Free Troposphere : Insights From Atmospheric Tomography (ATom), Journal of Geophysical Research : Atmospheres, 125, e2019JD031685, https://doi.org/10.1029/2019JD031685, 2019.

Brune, W. H., Miller, D. O., Thames, A. B., Brosius, A. L., Barletta, B., Blake, D. R., Blake, N. J., Chen, G., Choi, Y., Crawford, J. H., Digangi, J. P., Diskin, G., Fried, A., Hall, S. R., Hanisco, T. F., Huey, G. L., Hughes, S. C., Kim, M., Meinardi, S., Montzka, D. D., Pusede, S. E., Schroeder, J. R., Teng, A., Tanner, D. J., Ullmann, K., Walega, J., Weinheimer, A., Wisthaler, A., and Wennberg, P. O.: Observations of atmospheric oxidation and ozone production in South Korea, Atmos Environ, 269, 118854, https://doi.org/10.1016/j.atmosenv.2021.118854, 2022.

Burkholder, J. B., Sander, S. P., Abbatt, J. P. D., Barker, J. R., Cappa, C. D., Crounse, J. D., Dibble, T. S., Huie, R. E., Kolb, C. E., Kurylo, M. J., Orkin, V. L., Percival, C. J., Wilmouth, D. M., and Wine, P. H.: Chemical Kinetics and Photochemical Data for Use in Atmospheric Studies, Evaluation No. 19, Pasadena, CA, USA, 2020.

Butkovskaya, N. I., Pouvesle, N., Kukui, A., and Le Bras, G.: Mechanism of the OH-Initiated Oxidation of Glycolaldehyde over the Temperature Range 233−296 K, J Phys Chem A, 110, 13492–13499, https://doi.org/10.1021/jp064993k, 2006.

Coggon, M. M., Stockwell, C. E., Claflin, M. S., Pfannerstill, E. Y., Lu, X., Gilman, J. B., Marcantonio, J., Cao, C., Bates, K., Gkatzelis, G. I., Lamplugh, A., Katz, E. F., Arata, C., Apel, E. C., Hornbrook, R. S., Piel, F., Majluf, F., Blake, D. R., Wisthaler, A., Canagaratna, M., Lerner, B. M., Goldstein, A. H., Mak, J. E., and Warneke, C.: Identifying and correcting interferences to PTR-ToF- MS measurements of isoprene and other urban volatile organic compounds, Atmos Meas Tech, 17, 801–825, https://doi.org/10.5194/amt-17-801-2024, 2024.

Cohen, A. J., Brauer, M., Burnett, R., Anderson, H. R., Frostad, J., Estep, K., Balakrishnan, K., Brunekreef, B., Dandona, L., Dandona, R., Feigin, V., Freedman, G., Hubbell, B., Jobling, A., Kan, H., Knibbs, L., Liu, Y., Martin, R., Morawska, L., Pope, C. A., Shin, H., Straif, K., Shaddick, G., Thomas, M., van Dingenen, R., van Donkelaar, A., Vos, T., Murray, C. J. L., and Forouzanfar, M. H.: Estimates and 25-year trends of the global burden of disease attributable to ambient air pollution: an analysis of data from the Global Burden of Diseases Study 2015, The Lancet, 389, 1907–1918, https://doi.org/10.1016/S0140-6736(17)30505-6, 2017.

Colombi, N. K., Jacob, D. J., Yang, L. H., Zhai, S., Shah, V., Grange, S. K., Yantosca, R. M., Kim, S., and Liao, H.: Why is ozone in South Korea and the Seoul metropolitan area so high and increasing?, Atmos Chem Phys, 23, 4031–4044, https://doi.org/10.5194/acp-23-4031-2023, 2023.

Crawford, J. H., Ahn, J. Y., Al-Saadi, J., Chang, L., Emmons, L. K., Kim, J., Lee, G., Park, J. H., Park, R. J., Woo, J. H., Song, C. K., Hong, J. H., Hong, Y. D., Lefer, B. L., Lee, M., Lee, T., Kim, S., Min, K. E., Yum, S. S., Shin, H. J., Kim, Y. W., Choi, J. S., Park, J. S., Szykman, J. J., Long, R. W., Jordan, C. E., Simpson, I. J., Fried, A., Dibb, J. E., Cho, S. Y., and Kim, Y. P.: The Korea-United States air quality (KORUS-AQ) field study, Elementa, 9, 1–27, https://doi.org/10.1525/elementa.2020.00163, 2021.

Crounse, J., McKinney, K. A., Kwan, A. J., and Wennberg, P. O.: Measurement of gas-phase hydroperoxides by chemical ionization mass spectrometry, Anal Chem, 78, 6726–6732, https://doi.org/doi:10.1021/ac0604235, 2006.

Day, D. A., Wooldridge, P. J., Dillon, M. B., Thornton, J. A., and Cohen, R. C.: A thermal dissociation laser-induced fluorescence instrument for in situ detection of $NO_2$, peroxy nitrates, alkyl nitrates, and $HNO_3$, Journal of Geophysical Research-Atmospheres, 107, 4046, https://doi.org/10.1029/2001JD000779, 2002.

Day, D. A., Campuzano-Jost, P., Nault, B. A., Palm, B. B., Hu, W., Guo, H., Wooldridge, P. J., Cohen, R. C., Docherty, K. S., Huffman, J. A., De Sá, S. S., Martin, S. T., and Jimenez, J. L.: A systematic re-evaluation of methods for quantification of bulk particle-phase organic nitrates using real-Time aerosol mass spectrometry, Atmos Meas Tech, 15, 459–483, https://doi.org/10.5194/amt-15-459-2022, 2022.

Diskin, G. S., Podolske, J. R., Sachse, G. W., and Slate, T. A.: Open-path airborne tunable diode laser hygrometer, in: Diode Lasers and Applications in Atmospheric Sensing, edited by: Fried, A.,

Proceedings of the Society of Photo-Optical Instrumentation Engineers (SPIE), 4817, 196–204, https://doi.org/doi:10.1117/12.453736, 2002.

Espada, C. and Shepson, P. B.: The production of organic nitrates from atmospheric oxidation of ethers and glycol ethers, Int J Chem Kinet, 37, 686–699, https://doi.org/10.1002/kin.20121, 2005.

Faloona, I. C., Tan, D., Lesher, R. L., Hazen, N. L., Frame, C. L., Simpas, J. B., Harder, H., Martinez, M., Di Carlo, P., Ren, X., and Brune, W. H.: A Laser-induced Fluorescence Instrument for Detecting Tropospheric OH and $HO_2$ : Characteristics and Calibration, J Atmos Chem, 47, 139–167, https://doi.org/10.1023/B:JOCH.0000021036.53185.0e, 2004.

Farmer, D. K., Perring, A. E., Wooldridge, P. J., Blake, D. R., Baker, A., Meinardi, S., Huey, L. G., Tanner, D., Vargas, O., and Cohen, R. C.: Impact of organic nitrates on urban ozone production, Atmos Chem Phys, 11, 4085–4094, https://doi.org/10.5194/acp-11-4085-2011, 2011.

Fisher, J. A., Jacob, D. J., Travis, K. R., Kim, P. S., Marais, E. A., Miller, C. C., Yu, K., Zhu, L., Yantosca, R. M., Sulprizio, M. P., Mao, J., Wennberg, P. O., Crounse, J. D., Teng, A. P., Nguyen, T. B., Clair, J. M. S., Cohen, R. C., Romer, P., Nault, B. A., Wooldridge, P. J., Jimenez, J. L., Campuzano-Jost, P., Day, D. A., Hu, W., Shepson, P. B., Xiong, F., Blake, D. R., Goldstein, A. H., Misztal, P. K., Hanisco, T. F., Wolfe, G. M., Ryerson, T. B., Wisthaler, A., and Mikoviny, T.: Organic nitrate chemistry and its implications for nitrogen budgets in an isoprene- and monoterpene-rich atmosphere: Constraints from aircraft ($SEAC^4RS$) and ground-based (SOAS) observations in the Southeast US, Atmos Chem Phys, 16, https://doi.org/10.5194/acp-16-5969-2016, 2016.

Fried, A., Walega, J., Weibring, P., Richter, D., Simpson, I. J., Blake, D. R., Blake, N. J., Meinardi, S., Barletta, B., Hughes, S. C., Crawford, J. H., Diskin, G., Barrick, J., Hair, J., Fenn, M., Wisthaler, A., Mikoviny, T., Woo, J., Park, M., Kim, J., Min, K., Jeong, S., Wennberg, P. O., Kim, M. J., Crounse, J. D., Teng, A. P., Bennett, R., Yang-martin, M., Shook, M. A., Huey, G., Tanner, D., Knote, C., and Kim, J.: Airborne formaldehyde and volatile organic compound measurements over the Daesan petrochemical complex on Korea's northwest coast during the Korea-United States Air Quality study : Estimation of emission fluxes and effects on air quality, Elementa: Science of the Anthropocene, 8, 1, https://doi.org/10.1525/elementa.2020.121, 2020.

Galloway, M. M., Huisman, A. J., Yee, L. D., Chan, A. W. H., Loza, C. L., Seinfeld, J. H., and Keutsch, F. N.: Yields of oxidized volatile organic compounds during the OH radical initiated oxidation of isoprene, methyl vinyl ketone, and methacrolein under high-$NO_x$ conditions, Atmos Chem Phys, 11, https://doi.org/10.5194/acp-11-10779-2011, 2011.

Gaudel, A., Cooper, O. R., Ancellet, G., Barret, B., Boynard, A., Burrows, J. P., Clerbaux, C., Coheur, P. F., Cuesta, J., Cuevas, E., Doniki, S., Dufour, G., Ebojie, F., Foret, G., Garcia, O., Granados-Muñoz, M. J., Hannigan, J. W., Hase, F., Hassler, B., Huang, G., Hurtmans, D., Jaffe, D., Jones, N., Kalabokas, P., Kerridge, B., Kulawik, S., Latter, B., Leblanc, T., Le Flochmoën, E., Lin, W., Liu, J., Liu, X., Mahieu, E., McClure-Begley, A., Neu, J. L., Osman, M., Palm, M., Petetin, H., Petropavlovskikh, I., Querel, R., Rahpoe, N., Rozanov, A., Schultz, M. G., Schwab, J., Siddans, R., Smale, D., Steinbacher, M., Tanimoto, H., Tarasick, D. W., Thouret, V., Thompson, A. M., Trickl, T., Weatherhead, E., Wespes, C., Worden, H. M., Vigouroux, C., Xu, X., Zeng, G., and Ziemke, J.: Tropospheric Ozone Assessment Report: Present-day distribution and trends of tropospheric ozone relevant to climate and global atmospheric chemistry model evaluation, Elementa, 6, https://doi.org/10.1525/elementa.291, 2018.

907 Gil, J., Kim, J., Lee, M., Lee, G., Ahn, J., Soo, D., Jung, J., Cho, S., Whitehill, A., Szykman, J.,
908 and Lee, J.: Characteristics of HONO and its impact on $O_3$ formation in the Seoul Metropolitan
909 Area during the Korea-US Air Quality study, Atmos Environ, 247, 118182,
910 https://doi.org/10.1016/j.atmosenv.2020.118182, 2021.

911 Gkatzelis, G. I., Coggon, M. M., Mcdonald, B. C., Peischl, J., Aikin, K. C., Gilman, J. B., Trainer,
912 M., and Warneke, C.: Identifying Volatile Chemical Product Tracer Compounds in U.S. Cities,
913 Enviromental Science & Technology, 55, 188–199, https://doi.org/10.1021/acs.est.0c05467, 2021.

914 González-Sánchez, J. M., Brun, N., Wu, J., Ravier, S., and Clément, J.: On the importance of
915 multiphase photolysis of organic nitrates on their global atmospheric removal, Atmos Chem Phys,
916 23, 5851–5866, https://doi.org/10.5194/acp-23-5851-2023, 2023.

917 de Gouw, J. A., Middlebrook, A. M., Warneke, C., Goldan, P. D., Kuster, W. C., Roberts, J. M.,
918 Fehsenfeld, F. C., Worsnop, D. R., Canagaratna, M. R., Pszenny, A. A. P., Keene, W. C.,
919 Marchewka, M. L., Bertman, S. B., and Bates, T. S.: Budget of organic carbon in a polluted
920 atmosphere: Results from the New England Air Quality Study in 2002, Journal of Geophysical
921 Research: Atmospheres, 110, D16305, https://doi.org/10.1029/2004JD005623, 2005.

922 de Gouw, J. A., Gilman, J. B., Borbon, A., Warneke, C., Kuster, W. C., Goldan, P. D., Holloway,
923 J. S., Peischl, J., Ryerson, T. B., Parrish, D. D., Gentner, D. R., Goldstein, A. H., and Harley, R.
924 A.: Increasing atmospheric burden of ethanol in the United States, Geophys Res Lett, 39, L15803,
925 https://doi.org/10.1029/2012GL052109, 2012.

926 de Gouw, J. A., Gilman, J. B., Kim, S.-W., Alvarez, S. L., Dusanter, S., Graus, M., Griffith, S. M.,
927 Isaacman-VanWertz, G., Kuster, W. C., Lefer, B. L., Lerner, B. M., McDonald, B. C.,
928 Rappenglück, B., Roberts, J. M., Stevens, P. S., Stutz, J., Thalman, R., Veres, P. R., Volkamer, R.,
929 Warneke, C., Washenfelder, R. A., and Young, C. J.: Chemistry of Volatile Organic Compounds
930 in the Los Angeles Basin: Formation of Oxygenated Compounds and Determination of Emission
931 Ratios, Journal of Geophysical Research: Atmospheres, 123, 2298–2319,
932 https://doi.org/10.1002/2017JD027976, 2018.

933 Griffith, S. M., Hansen, R. F., Dusanter, S., Michoud, V., Gilman, J. B., Kuster, W. C., Veres, P.
934 R., Graus, M., de Gouw, J. A., Roberts, J., Young, C., Washenfelder, R., Brown, S. S., Thalman,
935 R., Waxman, E., Volkamer, R., Tsai, C., Stutz, J., Flynn, J. H., Grossberg, N., Lefer, B., Alvarez,
936 S. L., Rappenglueck, B., Mielke, L. H., Osthoff, H. D., and Stevens, P. S.: Measurements of
937 hydroxyl and hydroperoxy radicals during CalNex-LA: Model comparisons and radical budgets,
938 Journal of Geophysical Research: Atmospheres, 121, 4211–4232,
939 https://doi.org/10.1002/2015JD024358, 2016.

940 Grosjean, D., Grosjean, E., and Gertler, A. W.: On-Road Emissions of Carbonyls from Light-Duty
941 and Heavy-Duty Vehicles, Enviromental Science & Technology, 35, 45–53,
942 https://doi.org/10.1021/es001326a, 2002.

943 Hansen, R. F., Griffith, S. M., Dusanter, S., Gilman, J. B., Graus, M., Kuster, W. C., Veres, P. R.,
944 de Gouw, J. A., Warneke, C., Washenfelder, R. A., Young, C. J., Brown, S. S., Alvarez, S. L.,
945 Flynn, J. H., Grossberg, N. E., Lefer, B., Rappenglueck, B., and Stevens, P. S.: Measurements of
946 Total OH Reactivity During CalNex-LA, Journal of Geophysical Research: Atmospheres, 126,
947 e2020JD032988, https://doi.org/10.1029/2020JD032988, 2021.

948 Hurst Bowman, J., Barket, D. J., and Shepson, P. B.: Atmospheric chemistry of nonanal,
949 Enviromental Science & Technology, 37, 2218–2225, 2003.

Jenkin, M. E., Young, J. C., and Rickard, A. R.: The MCM v3.3.1 degradation scheme for isoprene, Atmos Chem Phys, 15, 11433–11459, https://doi.org/10.5194/acp-15-11433-2015, 2015.

Jo, D. S., Emmons, L. K., Callaghan, P., Tilmes, S., and Woo, J.: Comparison of Urban Air Quality Simulations During the KORUS-AQ Campaign With Regionally Refined Versus Global Uniform Grids in the Multi-Scale Infrastructure for Chemistry and Aerosols (MUSICA) Version 0, J Adv Model Earth Syst, 15, e2022MS003458, https://doi.org/10.1029/2022MS003458, 2023.

Jordan, C. E., Crawford, J. H., Beyersdorf, A. J., Eck, T. F., Halliday, H. S., Nault, B. A., Chang, L. S., Park, J. S., Park, R., Lee, G., Kim, H., Ahn, J. Y., Cho, S., Shin, H. J., Lee, J. H., Jung, J., Kim, D. S., Lee, M., Lee, T., Whitehill, A., Szykman, J., Schueneman, M. K., Campuzano-Jost, P., Jimenez, J. L., DiGangi, J. P., Diskin, G. S., Anderson, B. E., Moore, R. H., Ziemba, L. D., Fenn, M. A., Hair, J. W., Kuehn, R. E., Holz, R. E., Chen, G., Travis, K., Shook, M., Peterson, D. A., Lamb, K. D., and Schwarz, J. P.: Investigation of factors controlling PM2.5 variability across the South Korean Peninsula during KORUS-AQ, Elementa, 8, https://doi.org/10.1525/elementa.424, 2020.

Kabir, M., Jagiella, S., and Zabel, F.: Thermal Stability of n-Acyl Peroxynitrates, Int J Chem Kinet, 46, 462–469, https://doi.org/10.1002/kin.20862, 2014.

Kenagy, H. S., Sparks, T. L., Ryerson, T. B., Blake, D. R., and Cohen, R. C.: Evidence of Nighttime Production of Organic Nitrates During SEAC$^4$RS, FRAPPE, and KORUS-AQ, Geophys Res Lett, 47, e2020GL087860, https://doi.org/10.1029/2020GL087860, 2020.

Kenagy, H. S., Romer Present, P. S., Wooldridge, P. J., Nault, B. A., Campuzano-Jost, P., Day, D. A., Jimenez, J. L., Zare, A., Pye, H. O. T., Yu, J., Song, C. H., Blake, D. R., Woo, J. H., Kim, Y., and Cohen, R. C.: Contribution of Organic Nitrates to Organic Aerosol over South Korea during KORUS-AQ, Environ Sci Technol, 55, 16326–16338, https://doi.org/10.1021/acs.est.1c05521, 2021.

Kim, D., Cho, C., Jeong, S., Lee, S., Nault, B. A., Campuzano-jost, P., Day, D. A., Schroder, J. C., Jimenez, J. L., Volkamer, R., Pusede, S. E., Hall, S. R., Ullmann, K., Huey, L. G., Tanner, D. J., and Dibb, J.: Field observational constraints on the controllers in glyoxal (CHOCHO) reactive uptake to aerosol, Atmos Chem Phys, 22, 805–821, https://doi.org/10.5194/acp-22-805-2022, 2022a.

Kim, H., Zhang, Q., and Heo, J.: Influence of Intense secondary aerosol formation and long-range transport on aerosol chemistry and properties in the Seoul Metropolitan Area during spring time : Results from KORUS-AQ, Atmos. Chem. Phys., 18, 7149–7168, https://doi.org/10.51944/acp-2017-947, 2018.

Kim, H., Park, R. J., Kim, S., Brune, W. H., Diskin, G. S., Fried, A., Hall, S. R., Weinheimer, A. J., Wennberg, P., Wisthaler, A., Blake, D. R., and Ullmann, K.: Observed versus simulated OH reactivity during KORUS-AQ campaign : Implications for emission inventory and chemical environment in East Asia, Elementa, 10, 1–26, 2022b.

Kim, J., Lee, J., Han, J., Choi, J., Kim, D.-G., Park, J., and Lee, G.: Long-term Assessment of Ozone Nonattainment Changes in South Korea Compared to US, and EU Ozone Guidelines, Asian Journal of Atmospheric Environment, 15, 20–32, https://doi.org/10.5572/ajae.2021.098, 2021.

Kim, S., Huey, L. G., Stickel, R. E., Tanner, D. J., Crawford, J. H., Olson, J. R., Chen, G., Brune, W. H., Ren, X., Lesher, R., Wooldridge, P. J., Bertram, T. H., Perring, A., Cohen, R. C., Lefer, B.

L., Shetter, R. E., Avery, M., Diskin, G., and Sokolik, I.: Measurement of HO2NO2 in the free troposphere during the Intercontinental Chemical Transport Experiment–North America 2004, Journal of Geophysical Research: Atmospheres, 112, D12S01, https://doi.org/10.1029/2006JD007676, 2007.

Kim, S., Sanchez, D., Wang, M., Seco, R., Jeong, D., Hughes, S., Barletta, B., Blake, D. R., Jung, J., Kim, D., Lee, G., Lee, M., Ahn, J., Lee, S.-D., Cho, G., Sung, M.-Y., Lee, Y.-H., Kim, D. B., Kim, Y., Woo, J.-H., Jo, D., Park, R., Park, J.-H., Hong, Y.-D., Hong, J.-H., Zhang, D. Y., Liu, J. J., Li, B. J., Davis, D. L., Bell, M. L., Fletcher, T., Haagen-Smit, A. J., Blacet, F. E., Edinger, J. G., Yum, S. S., Roberts, G., Kim, J. H., Song, K. Y., Kim, D. Y., Lim, Y. J., Armendariz, A., Son, Y. S., Kim, J. C., Kim, S., Kim, S. Y., Lee, M., Shim, H., Wolfe, G. M., Guenther, A. B., He, A., Hong, Y., Han, J., Kim, S., Lee, M., Kim, S., Choi, S., Seok, S., Kim, S., Kim, S. Y., Jiang, X. Y., Lee, M., Turnipseed, A., Guenther, A., Kim, J. C., Lee, S. J., Kim, S., Lee, K. Y., Kwak, K. H., Ryu, Y. H., Lee, S. H., Baik, J. J., Ryu, Y. H., Baik, J. J., Kwak, K. H., Kim, S., Moon, N., Bao, H., Shrestha, K. L., Kondo, A., Kaga, A., Inoue, Y., Ran, L., Zhao, C. S., Xu, W. Y., Lu, X. Q., Han, M., Lin, W. L., Yan, P., Xu, X. B., Deng, Z. Z., Ma, N., Liu, P. F., Yu, J., Liang, W. D., Chen, L. L., Geng, F., Tie, X., Guenther, A., Li, G., et al.: OH reactivity in urban and suburban regions in Seoul, South Korea – an East Asian megacity in a rapid transition, Faraday Discuss., 189, 231–251, https://doi.org/10.1039/C5FD00230C, 2016.

KORUS-AQ Science Team: KORUS-AQ Data, [Dataset], NASA Langley Research Center., https://doi.org/10.5067/Suborbital/KORUSAQ/DATA01, 2023.

LaFranchi, B. W., Wolfe, G. M., Thornton, J. a., Harrold, S. a., Browne, E. C., Min, K. E., Wooldridge, P. J., Gilman, J. B., Kuster, W. C., Goldan, P. D., DeGouw, J. a., McKay, M., Goldstein, a. H., Ren, X. R., Mao, J. Q., Cohen, R. C., de Gouw, J. a., Welsh-Bon, D., Chen, Z., and Brune, W. H.: Closing the peroxy acetyl (PA) radical budget: Observations of acyl peroxy nitrates (PAN, PPN and MPAN) during BEARPEX 2009, Abstracts of Papers of the American Chemical Society, 9, 289, https://doi.org/10.5194/acp-9-7623-2009, 2009.

Lee, Y. R., Huey, L. G., Tanner, D. J., Takeuchi, M., Qu, H., Liu, X., Ng, N. L., Crawford, J. H., Fried, A., Richter, D., Simpson, I. J., Blake, D. R., Blake, N. J., Meinardi, S., Kim, S., Diskin, G. S., Digangi, J. P., Choi, Y., Pusede, S. E., Wennberg, P. O., Kim, M. J., Crounse, J. D., Teng, A. P., Cohen, R. C., Romer, P. S., Brune, W., Wisthaler, A., Mikoviny, T., Jimenez, J. L., Campuzano-Jost, P., Nault, B. A., Weinheimer, A., Hall, S. R., and Ullmann, K.: An investigation of petrochemical emissions during KORUS-AQ: Ozone production, reactive nitrogen evolution, and aerosol production, Elementa, 10, 1–24, https://doi.org/10.1525/elementa.2022.00079, 2022.

Ling, Z., Xie, Q., Shao, M., Wang, Z., Wang, T., Guo, H., and Wang, X.: Formation and sink of glyoxal and methylglyoxal in a polluted subtropical environment: Observation-based photochemical analysis and impact evaluation, Atmos Chem Phys, 20, 11451–11467, https://doi.org/10.5194/acp-20-11451-2020, 2020.

Liu, Y., Yuan, B., Li, X., Shao, M., Lu, S., Li, Y., Chang, C., Wang, Z., Hu, W., Huang, X., He, L., Zeng, L., Hu, M., and Zhu, T.: Impact of pollution controls in Beijing on atmospheric oxygenated volatile organic compounds ( OVOCs ) during the 2008 Olympic Games : observation and modeling implications, Atmos Chem Phys, 15, 3045–3062, https://doi.org/10.5194/acp-15-3045-2015, 2015.

Lyu, X. P., Zeng, L. W., Guo, H., Simpson, I. J., Ling, Z. H., Wang, Y., Murray, F., Louie, P. K. K., Saunders, S. M., Lam, S. H. M., and Blake, D. R.: Evaluation of the effectiveness of air pollution control measures in Hong Kong, Environmental Pollution, 220, 87–94, https://doi.org/10.1016/j.envpol.2016.09.025, 2017.

Ma, P. K., Zhao, Y., Robinson, A. L., Worton, D. R., Goldstein, A. H., Ortega, A. M., Jimenez, J.-L., Zotter, P., Prévôt, A. S. H., Szidat, S., and Hayes, P. L.: Evaluating the impact of new observational constraints on P-S/IVOC emissions, multi-generation oxidation, and chamber wall losses on SOA modeling for Los Angeles, CA, Atmos Chem Phys, 17, 9237–9259, https://doi.org/10.5194/acp-17-9237-2017, 2017.

Ma, X., Tan, Z., Lu, K., Yang, X., Chen, X., Wang, H., Chen, S., Fang, X., Li, S., Li, X., Liu, J., Liu, Y., Lou, S., Qiu, W., and Wang, H.: OH and HO 2 radical chemistry at a suburban site during the EXPLORE-YRD campaign in 2018, Atmos Chem Phys, 22, 7005–7028, https://doi.org/10.5194/acp-22-7005-2022, 2022.

Magneron, I., Mellouki, A., Le Bras, G., Moortgat, G. K., Horowitz, A., and Wirtz, K.: Photolysis and OH-Initiated Oxidation of Glycolaldehyde under Atmospheric Conditions, J Phys Chem A, 109, 4552–4561, https://doi.org/10.1021/jp044346y, 2005.

Mao, J., Ren, X., Brune, W. H., Olson, J. R., Crawford, J. H., Fried, a., Huey, L. G., Cohen, R. C., Heikes, B., Singh, H. B., Blake, D. R., Sachse, G. W., Diskin, G. S., Hall, S. R., and Shetter, R. E.: Airborne measurement of OH reactivity during INTEX-B, Atmos Chem Phys, 9, 163–173, https://doi.org/10.5194/acp-9-163-2009, 2009.

McDonald, B. C., de Gouw, J. A., Gilman, J. B., Jathar, S. H., Akherati, A., Cappa, C. D., Jimenez, J. L., Lee-Taylor, J., Hayes, P. L., McKeen, S. A., Cui, Y. Y., Kim, S.-W., Gentner, D. R., Isaacman-VanWertz, G., Goldstein, A. H., Harley, R. A., Frost, G. J., Roberts, J. M., Ryerson, T. B., and Trainer, M.: Volatile chemical products emerging as largest petrochemical source of urban organic emissions, Science, 359, 760–764, https://doi.org/10.1126/science.aaq0524, 2018.

Mellouki, A., Wallington, T. J., and Chen, J.: Atmospheric chemistry of oxygenated volatile organic compounds: Impacts on air quality and climate, Chem Rev, 115, 3984–4014, https://doi.org/10.1021/cr500549n, 2015.

Millet, D. B., Apel, E., Henze, D. K., Hill, J., Marshall, J. D., Singh, H. B., and Tessum, C. W.: Natural and Anthropogenic Ethanol Sources in North America and Potential Atmospheric Impacts of Ethanol Fuel Use, Enviromental Science & Technology, 46, 8484–8492, 2012.

Min, K.-E., Washenfelder, R. a., Dubé, W. P., Langford, a. O., Edwards, P. M., Zarzana, K. J., Stutz, J., Lu, K., Rohrer, F., Zhang, Y., and Brown, S. S.: A broadband cavity enhanced absorption spectrometer for aircraft measurements of glyoxal, methylglyoxal, nitrous acid, nitrogen dioxide, and water vapor, Atmos Meas Tech, 9, 423–440, https://doi.org/10.5194/amt-9-423-2016, 2016.

Müller, M., Mikoviny, T., Feil, S., Haidacher, S., Hanel, G., Hartungen, E., Jordan, A., Märk, L., Mutschlechner, P., Schottkowsky, R., Sulzer, P., Crawford, J. H., and Wisthaler, A.: A compact PTR-ToF-MS instrument for airborne measurements of volatile organic compounds at high spatiotemporal resolution, Atmos Meas Tech, 7, 3763–3772, https://doi.org/10.5194/amt-7-3763-2014, 2014.

Nault, B. A., Campuzano-Jost, P., Day, D. A., Schroder, J. C., Anderson, B., Beyersdorf, A. J., Blake, D. R., Brune, W. H., Choi, Y., Corr, C. A., de Gouw, J. A., Dibb, J., DiGangi, J. P., Diskin,

G. S., Fried, A., Huey, L. G., Kim, M. J., Knote, C. J., Lamb, K. D., Lee, T., Park, T., Pusede, S. E., Scheuer, E., Thornhill, K. L., Woo, J.-H., and Jimenez, J. L.: Secondary organic aerosol production from local emissions dominates the organic aerosol budget over Seoul, South Korea, during KORUS-AQ, Atmos Chem Phys, 18, 17769–17800, https://doi.org/10.5194/acp-18-17769-2018, 2018.

Nihill, K. J., Ye, Q., Majluf, F., Krechmer, J. E., Canagaratna, M. R., and Kroll, J. H.: Influence of the $NO/NO_2$ Ratio on Oxidation Product Distributions under High-NO Conditions, Environ Sci Technol, 55, 6594–6601, https://doi.org/10.1021/acs.est.0c07621, 2021.

Orlando, J. J. and Tyndall, G. S.: Laboratory studies of organic peroxy radical chemistry: an overview with emphasis on recent issues of atmospheric significance, Chem Soc Rev, 41, 6294–6317, https://doi.org/10.1039/c2cs35166h, 2012.

Park, R. J., Oak, Y. J., Emmons, L. K., Kim, C. H., Pfister, G. G., Carmichael, G. R., Saide, P. E., Cho, S. Y., Kim, S., Woo, J. H., Crawford, J. H., Gaubert, B., Lee, H. J., Park, S. Y., Jo, Y. J., Gao, M., Tang, B., Stanier, C. O., Shin, S. S., Park, H. Y., Bae, C., and Kim, E.: Multi-model intercomparisons of air quality simulations for the KORUS-AQ campaign, Elementa, 9, 1–29, https://doi.org/10.1525/elementa.2021.00139, 2021.

Perring, A. E., Bertram, T. H., Farmer, D. K., Wooldridge, P. J., Dibb, J., Blake, N. J., Blake, D. R., Singh, H. B., Fuelberg, H., Diskin, G., Sachse, G., and Cohen, R. C.: The production and persistence of $\Sigma RONO_2$ in the Mexico City plume, Atmos Chem Phys, 10, 7215–7229, https://doi.org/10.5194/acp-10-7215-2010, 2010.

Perring, A. E., Pusede, S. E., and Cohen, R. C.: An observational perspective on the atmospheric impacts of alkyl and multifunctional nitrates on ozone and secondary organic aerosol., Chem Rev, 113, 5848–70, https://doi.org/10.1021/cr300520x, 2013.

Peterson, D. A., Hyer, E. J., Han, S. O., Crawford, J. H., Park, R. J., Holz, R., Kuehn, R. E., Eloranta, E., Knote, C., Jordan, C. E., and Lefer, B. L.: Meteorology influencing springtime air quality, pollution transport, and visibility in Korea, Elementa, 7, https://doi.org/10.1525/elementa.395, 2019.

Picquet-Varrault, B., Suarez-Bertoa, R., Duncianu, M., Cazaunau, M., Pangui, E., David, M., Doussin, J., Cnrs, U. M. R., Créteil, U. P., Paris, U. De, Pierre, I., and Laplace, S.: Photolysis and oxidation by OH radicals of two carbonyl nitrates : 4-nitrooxy-2-butanone and 5-nitrooxy-2-pentanone, Atmos Chem Phys, 20, 487–498, https://doi.org/10.5194/acp-20-487-2020, 2020.

Rao, H., Fullana, A., Sidhu, S., and Carbonell-barrachina, Á. A.: Emissions of volatile aldehydes from heated cooking oils, Food Chem, 120, 59–65, https://doi.org/10.1016/j.foodchem.2009.09.070, 2010.

Ren, X., Duin, D. Van, Cazorla, M., Chen, S., Mao, J., Zhang, L., Brune, W. H., Flynn, J. H., Grossberg, N., Lefer, B. L., Rappenglück, B., Wong, K. W., Tsai, C., Stutz, J., Dibb, J. E., Jobson, B. T., Luke, W. T., and Kelley, P.: Atmospheric oxidation chemistry and ozone production : Results from SHARP 2009 in Houston, Texas, Journal of Geophysical Research: Atmospheres, 118, 5770–5780, https://doi.org/10.1002/jgrd.50342, 2013.

Richter, D., Weibring, P., Walega, J. G., Fried, A., Spuler, S. M., and Taubman, M. S.: Compact highly sensitive multi-species airborne mid-IR spectrometer, Applied Physics B, 119, 119–131, https://doi.org/10.1007/s00340-015-6038-8, 2015.

Rosen, R. S., Wood, E. C., Wooldridge, P. J., Thornton, J. A., Day, D. A., Kuster, W., Williams, E. J., Jobson, B. T., and Cohen, R. C.: Observations of total alkyl nitrates during Texas Air Quality Study 2000 : Implications for $O_3$ and alkyl nitrate photochemistry, J Geophys Res, 109, D07303, https://doi.org/10.1029/2003JD004227, 2004.

Sachse, G. W., Hill, G. F., Wade, L. O., and Perry, M. G.: Fast-Response, High-Precision Carbon Monoxide Sensor using a Tunable Diode Laser Absorption Technique, Journal of Geophysical Research: Atmospheres, 92, 2071–2081, https://doi.org/doi:10.1029/JD092iD02p02071, 1987.

Sai, S., Ho, H., Yu, J. Z., Chu, K. W., Yeung, L. L., Sai, S., Ho, H., Yu, J. Z., Chu, K. W., and Yeung, L. L.: Carbonyl Emissions from Commercial Cooking Sources in Hong Kong Carbonyl Emissions from Commercial Cooking Sources in Hong Kong, J Air Waste Manage Assoc, 56, 1091–1098, https://doi.org/10.1080/10473289.2006.10464532, 2012.

Saunders, S. M., Jenkin, M. E., Derwent, R. G., and Pilling, M. J.: Protocol for the development of the Master Chemical Mechanism, MCM v3 (Part A): tropospheric degradation of non-aromatic volatile organic compounds, Atmos Chem Phys, 3, 161–180, https://doi.org/10.5194/acp-3-161-2003, 2003.

Schauer, J. J., Kleeman, M. J., Cass, G. R., and Simoneit, B. R. T.: Measurement of Emissions from Air Organic Compounds from Cooking with Seed Oils, Environ Sci Technol, 36, 567–575, https://doi.org/10.1021/es002053m, 2002.

von Schneidemesser, E., McDonald, B. C., Denier van der Gon, H., Crippa, M., Guizzardi, D., Borbon, A., Dominutti, P., Huang, G., Jansens-Maenhout, G., Li, M., Ou-Yang, C. F., Tisinai, S., and Wang, J. L.: Comparing Urban Anthropogenic NMVOC Measurements With Representation in Emission Inventories—A Global Perspective, Journal of Geophysical Research: Atmospheres, 128, https://doi.org/10.1029/2022JD037906, 2023.

Schroeder, J. R., Crawford, J. H., Ahn, J. Y., Chang, L., Fried, A., Walega, J., Weinheimer, A., Montzka, D. D., Hall, S. R., Ullmann, K., Wisthaler, A., Mikoviny, T., Chen, G., Blake, D. R., Blake, N. J., Hughes, S. C., Meinardi, S., Diskin, G., Digangi, J. P., Choi, Y., Pusede, S. E., Huey, G. L., Tanner, D. J., Kim, M., and Wennberg, P.: Observation-based modeling of ozone chemistry in the Seoul metropolitan area during the Korea-United States Air Quality Study (KORUS-AQ), Elementa, 8, https://doi.org/10.1525/elementa.400, 2020.

Seo, J., Park, D. R., Kim, J. Y., Youn, D., Lim, Y. Bin, and Kim, Y.: Effects of meteorology and emissions on urban air quality : a quantitative statistical approach to long-term records (1999 – 2016) in Seoul , South Korea, Atmos Chem Phys, 18, 16121–16137, 2018.

Shetter, R. E. and Müller, M.: Photolysis frequency measurements using actinic flux spectroradiometry during the PEM-Tropics mission: Instrumentation description and some results, Journal of Geophysical Research-Atmospheres, 104, 5647–5661, https://doi.org/10.1029/98JD01381, 1999.

Simpson, I. J., Blake, D. R., Blake, N. J., Meinardi, S., Barletta, B., Hughes, S. C., Fleming, L. T., Crawford, J. H., Diskin, G. S., Emmons, L. K., Fried, A., Guo, H., Peterson, D. A., Wisthaler, A., Woo, J., Barré, J., Gaubert, B., Kim, J., Kim, M. J., Kim, Y., Knote, C., Mikoviny, T., Sally, E., Schroeder, J. R., Wang, Y., Wennberg, P. O., and Zeng, L.: Characterization , sources and reactivity of volatile organic compounds ( VOCs ) in Seoul and surrounding regions during KORUS-AQ, Elementa: Science of the Anthropocene, 8, 37, https://doi.org/10.1525/elementa.434, 2020.

Sprengnether, M. M., Demerjian, K. L., Dransfield, T. J., Clarke, J. S., Anderson, J. G., and Donahue, N. M.: Rate Constants of Nine C6-C9 Alkanes with OH from 230 to 379 K: Chemical Tracers for [OH] , J Phys Chem A, 113, 5030–5038, https://doi.org/10.1021/jp810412m, 2009.

Tan, Z., Lu, K., Hofzumahaus, A., Fuchs, H., Bohn, B., Holland, F., Liu, Y., Rohrer, F., Shao, M., Sun, K., Wu, Y., Zeng, L., Zhang, Y., Zou, Q., Kiendler-Scharr, A., Wahner, A., and Zhang, Y.: Experimental budgets of OH, $HO_2$, and $RO_2$ radicals and implications for ozone formation in the Pearl River Delta in China 2014, Atmos Chem Phys, 19, 7129–7150, https://doi.org/10.5194/acp-19-7129-2019, 2019.

Teng, A. P., Crounse, J. D., Lee, L., St Clair, J. M., Cohen, R. C., and Wennberg, P. O.: Hydroxy nitrate production in the OH-initiated oxidation of alkenes, Atmos Chem Phys, 15, 4297–4316, https://doi.org/10.5194/acp-15-4297-2015, 2015.

Thornton, J. A., Wooldridge, P. J., and Cohen, R. C.: Atmospheric $NO_2$: In-situ laser-induced fluorescence detection at parts per trillion mixing ratios, Anal Chem, 72, 528–539, https://doi.org/doi:10.1021/ac9908905, 2000.

Travis, K. R., Crawford, J. H., Chen, G., Jordan, C. E., Nault, B. A., Kim, H., Jimenez, J. L., Campuzano-Jost, P., Dibb, J. E., Woo, J. H., Kim, Y., Zhai, S., Wang, X., McDuffie, E. E., Luo, G., Yu, F., Kim, S., Simpson, I. J., Blake, D. R., Chang, L., and Kim, M. J.: Limitations in representation of physical processes prevent successful simulation of PM2.5 during KORUS-AQ, Atmos Chem Phys, 22, 7933–7958, https://doi.org/10.5194/acp-22-7933-2022, 2022.

Tuite, K., Thomas, J. L., Veres, P. R., and Roberts, J. M.: Quantifying Nitrous Acid Formation Mechanisms Using Measured Vertical Profiles During the CalNex 2010 Campaign and 1D Column Modeling, Journal of Geophysical Research: Atmospheres, 126, e2021JD034689, https://doi.org/10.1029/2021JD034689, 2021.

Wang, W., Yuan, B., Peng, Y., Su, H., Cheng, Y., Yang, S., Wu, C., Qi, J., Bao, F., Huangfu, Y., Wang, C., Ye, C., Wang, Z., Wang, B., Wang, X., Song, W., Hu, W., Cheng, P., Zhu, M., Zheng, J., and Shao, M.: Direct observations indicate photodegradable oxygenated volatile organic compounds (OVOCs) as larger contributors to radicals and ozone production in the atmosphere, Atmos Chem Phys, 22, 4117–4128, https://doi.org/10.5194/acp-22-4117-2022, 2022.

Wargocki, P., Weschler, J., and Williams, J.: Assessment of aldehyde contributions to PTR-MS m/z 69.07 in indoor air measurements, Environmental Science: Atmospheres, Advance Ar, https://doi.org/10.1039/d3ea00055a, 2023.

Weinheimer, A. J., Walega, J. G., Ridley, B. A., Gary, B. L., Blake, D. R., Blake, N. J., Rowland, F. S., Sachse, G. W., Anderson, B. E., and Collins, J. E.: Meridional distributions of $NO_x$ , $NO_y$ , and other species in the lower stratosphere and upper troposphere during AASE II, Geophys Res Lett, 21, 2583–2586, https://doi.org/10.1029/94GL01897, 1994.

Whalley, L. K., Stone, D., Bandy, B., Dunmore, R., Hamilton, J. F., Hopkins, J., Lee, J. D., Lewis, A. C., and Heard, D. E.: Atmospheric OH reactivity in central London: observations, model predictions and estimates of in situ ozone production, Atmos Chem Phys, 16, 2109–2122, https://doi.org/10.5194/acp-16-2109-2016, 2016.

Whalley, L. K., Stone, D., Dunmore, R., Hamilton, J., Hopkins, J. R., Lee, J. D., Lewis, A. C., Williams, P., Kleffmann, J., Laufs, S., and Woodward-massey, R.: Understanding in situ ozone production in the summertime through radical observations and modelling studies during the Clean

air for London project ( ClearfLo ), Atmos Chem Phys, 18, 2547–2571, https://doi.org/10.5194/acp-18-2547-2018, 2018.

Whalley, L. K., Slater, E. J., Woodward-massey, R., Ye, C., Lee, J. D., Squires, F., Mehra, A., Worrall, S. D., Bacak, A., Bannan, T. J., Coe, H., and Percival, C. J.: Evaluating the sensitivity of radical chemistry and ozone formation to ambient VOCs and $NO_x$ in Beijing, Atmos Chem Phys, 21, 2125–2147, https://doi.org/10.5194/acp-21-2125-2021, 2021.

Wolfe, G. M., Marvin, M. R., Roberts, S. J., Travis, K. R., and Liao, J.: The Framework for 0-D Atmospheric Modeling (F0AM) v3.1, Geosci Model Dev, 9, 3309–3319, https://doi.org/10.5194/gmd-9-3309-2016, 2016.

Wooldridge, P. J., Perring, A. E., Bertram, T. H., Flocke, F. M., Roberts, J. M., Singh, H. B., Huey, L. G., Thornton, J. A., Wolfe, G. M., Murphy, J. G., Fry, J. L., Rollins, A. W., LaFranchi, B. W., and Cohen, R. C.: Total Peroxy Nitrates (ΣPNs) in the atmosphere: the Thermal Dissociation-Laser Induced Fluorescence (TD-LIF) technique and comparisons to speciated PAN measurements, Atmos Meas Tech, 3, 593–607, https://doi.org/DOI 10.5194/amt-3-593-2010, 2010.

Xu, Y., Feng, X., Chen, Y., Zheng, P., Hui, L., Chen, Y., Yu, J. Z., and Wang, Z.: Development of an enhanced method for atmospheric carbonyls and characterizing their roles in photochemistry in subtropical Hong Kong, Science of The Total Environment, 896, 165135, https://doi.org/10.1016/j.scitotenv.2023.165135, 2023.

Yang, G., Huo, J., Wang, L., Wang, Y., Wu, S., Yao, L., Fu, Q., and Wang, L.: Total OH Reactivity Measurements in a Suburban Site of Shanghai J, Journal of Geophysical Research: Atmospheres, 127, 1–20, https://doi.org/10.1029/2021JD035981, 2022.

Yeh, G. K. and Ziemann, P. J.: Alkyl nitrate formation from reactions of C8-C14 n-alkanes with OH radicals in the presence of NOx: Measured yields with essential corrections for gas-wall partitioning, Journal of Physical Chemistry A, 118, 8147–8157, https://doi.org/10.1021/jp500631v, 2014.

Yeo, M. J. and Kim, Y. P.: Long-term trends of surface ozone in Korea, J Clean Prod, 294, 125352, https://doi.org/10.1016/j.jclepro.2020.125352, 2021.

Yuan, B., Shao, M., de Gouw, J., Parrish, D. D., Lu, S., Wang, M., Zeng, L., Zhang, Q., Song, Y., Zhang, J., and Hu, M.: Volatile organic compounds (VOCs) in urban air: How chemistry affects the interpretation of positive matrix factorization (PMF) analysis, Journal of Geophysical Research: Atmospheres, 117, n/a-n/a, https://doi.org/10.1029/2012JD018236, 2012.

Zare, A., Romer, P. S., Nguyen, T., Keutsch, F. N., Skog, K., and Cohen, R. C.: A comprehensive organic nitrate chemistry: Insights into the lifetime of atmospheric organic nitrates, Atmos Chem Phys, 18, 15419–15436, https://doi.org/10.5194/acp-18-15419-2018, 2018.

Zhao, Y., Hennigan, C. J., May, A. A., Tkacik, D. S., De Gouw, J. A., Gilman, J. B., Kuster, W. C., Borbon, A., and Robinson, A. L.: Intermediate-volatility organic compounds: A large source of secondary organic aerosol, Environ Sci Technol, 48, 13743–13750, https://doi.org/10.1021/es5035188, 2014.

Zheng, W., Flocke, F. M., Tyndall, G. S., Swanson, A., Orlando, J. J., Roberts, J. M., Huey, L. G., and Tanner, D. J.: Characterization of a thermal decomposition chemical ionization mass spectrometer for the measurement of peroxy acyl nitrates (PANs) in the atmosphere, Atmos Chem Phys, 11, 6529–6547, https://doi.org/10.5194/acp-11-6529-2011, 2011.

Zhou, Z., Tan, Q., Deng, Y., Song, D., Wu, K., Zhou, X., Huang, F., Zeng, W., and Lu, C.: Compilation of emission inventory and source profile database for volatile organic compounds : A case study for Sichuan, China, Atmos Pollut Res, 11, 105–116, https://doi.org/10.1016/j.apr.2019.09.020, 2020.

## Tables

**Table 1.** Reactions described in text along with associated rate constants and references for those rate constants.

| | *Reaction* | *Reaction Rate* | *Reference* |
|---|---|---|---|
| R1a | $VOC+OH \xrightarrow{O_2} RO_2^{\cdot}$ | Varies | Atkinson (2003); Atkinson and Arey(2003); Atkinson et al. (2006); Bohn and Zetzsch (2012); Sprengnether et al. (2009) |
| R1b | $VOC+h\nu \xrightarrow{O_2} RO_2^{\cdot}$ | Varies/Measured | Shetter & Müller (1999) |
| R2a | $RO_2^{\cdot}+NO \rightarrow (1-\alpha)\ RO^{\cdot}+(1-\alpha)\ NO_2$ | $2.7\times10^{-11}\times\exp(390/T)$ | Burkholder et al. (2020) |
| R2b | $RO_2^{\cdot}+NO \rightarrow \alpha\ RONO_2$ | $2.7\times10^{-11}\times\exp(390/T)$ | Burkholder et al. (2020) |
| R3 | $NO_2+h\nu \rightarrow NO+O(^3P)$ | Measured on DC-8 | Shetter & Müller (1999) |
| R4 | $O(^3P)+O_2 \rightarrow O_3$ | $3.2\times10^{-11}\times\exp(67/T)$ | Saunders et al. (2003) |
| R5 | $RO^{\cdot}+O_2 \rightarrow R(O)+HO_2$ | Assumed Instantaneous | |
| R6 | $HO_2+NO \rightarrow OH+NO_2$ | $3.45\times10^{-12}\times\exp(270/T)$ | Saunders et al. (2003) |
| R7 | $RCHO+OH \xrightarrow{O_2} R(O)O_2^{\cdot}$ | Varies | Atkinson (2003); Atkinson and Arey (2003); Atkinson et al. (2006) |
| R8[a] | $R(O)O_2^{\cdot}+NO_2 \leftrightarrow R(O)O_2NO_2$ | F: $8.69\times10^{-12}$ $cm^3$ $molec.^{-1}$ $s^{-1}$<br>R: $4.30\times10^{-4}$ $s^{-1}$ | Burkholder et al. (2020) |
| R9 | $R(O)O_2+NO \rightarrow RO_2^{\cdot}+NO_2$ | $8.1\times10^{-12}\times\exp(270/T)$ | Burkholder et al. (2020) |
| R10 | $O_3+NO \rightarrow O_2+NO_2$ | $2.07\times10^{-12}\times(-1400/T)$ | Burkholder et al. (2020) |
| R11[b] | $OH+NO_2 \rightarrow HNO_3$ | $1.24\times10^{-11}$ $cm^3$ $molec.^{-1}$ $s^{-1}$ | Burkholder et al. (2020) |
| R12 | $O_3+h\nu \xrightarrow{H_2O} 2O(^1D)$ | hν measured on DC-8; $2.14\times10^{-10}$ $cm^3$ $molec.^{-1}$ $s^{-1}$ | Shetter & Müller (1999); Saunders et al. (2003) |
| R13 | $O_3+OH \rightarrow HO_2+O_2$ | $1.7\times10^{-12}\times\exp(-940/T)$ | Saunders et al. (2003) |
| R14 | $O_3+HO_2 \rightarrow OH+2O_2$ | $1.0\times10^{-14}\times\exp(-490/T)$ | Burkholder et al. (2020) |
| R15[b] | $HO_2+HO_2 \xrightarrow{H_2O} H_2O_2$ | $5.06\times10^{-12}$ $cm^3$ $molec.^{-1}$ $s^{-1}$ | Saunders et al. (2003) |
| R16 | $HO_2+RO_2 \rightarrow Products$ | $2.91\times10^{-13}\times\exp(1300/T)$ | Saunders et al. (2003) |
| R17 | $HO_2+OH \rightarrow Products$ | $4.80\times10^{-11}\times\exp(250/T)$ | Burkholder et al. (2020) |

| | | | |
|---|---|---|---|
| R18[b] | OH+NO → HONO | $7.40\times10^{-12}$ $cm^3$ $molec.^{-1}$ $s^{-1}$ | Burkholder et al. (2020) |
| R19 | $HO_2$+R(O)$O_2$ → Products | $4.30\times10^{-13}\times\exp(1040/T)$ | Burkholder et al. (2020) |

[a]Only showing forward (F) and reverse (R) rate constant at 298 K and 1013 hPa and being a termolecular reaction.

[b]Termolecular reaction; only showing rate at 298 K and 1013 hPa

**Table 2.** List of instruments, compounds measured, accuracy/precision, and associated references used in this study.

| Instrument | Species | References |
|---|---|---|
| University of California, Irvine, Whole Air Sampler (WAS) | Ethane, Ethene, Ethyne, Propane, Propene, i-Butane, n-Butane, 1-Butene, i-Butene, trans-2-Butene, cis-2-Butene i-Pentane, n-Pentane, 1,3-Butadiene, Isoprene, n-Hexane, n-Heptane, n-Octane, n-Nonane, n-Decane, 2,3-Dimethylbutane, 2-Methylpentane, 3-Methylpentane, Cyclopentane, Methylcyclopentane, Cyclohexane, Methylcyclohexane, Benzene, Toluene, m+p-Xylene, o-Xylene, Ethylbenzene, Styrene, i-Propylbenzene, n-Propylbenzene, 3-Ethyltoluene, 4-Ethyltoluene, 2-Ethyltoluene, 1,3,5-Trimethylbenzene, 1,2,4-Trimethylbenzene, 1,2,3-Trimethylbenzene, α-Pinene, β-Pinene, Methyl nitrate, Ethyl nitrate, i-Propyl nitrate, n-Propyl nitrate, 2-Butyl nitrate, 3-Pentyl nitrate, 2-Pentyl nitrate, 3-Methyl-2-Butyl nitrate | Simpson et al. (2020) |
| The Pennsylvania State University Airborne Tropospheric Hydrogen Oxides Sensor (ATHOS) | OH, $HO_2$, OH Reactivity | Faloona et al. (2004), Mao et al. (2009), Brune et al. (2019) |
| University of California, Berkeley, Thermal Dissociation-Laser Induced Fluorescence (TD-LIF) | $NO_2$, ΣPNs, ΣANs | Thornton et al. (2000), Day et al. (2002), Wooldridge et al. (2010) |
| NASA Langley Diode Laser Hygrometer (DLH) | $H_2O$ | Diskin et al. (2002) |
| NASA Langley Diode Laser Spectrometer Measurements (DACOM) | CO, $CH_4$ | Sachse et al. (1987) |
| University of Colorado, Boulder, Compact Atmospheric Multi-species Spectrometer (CAMS) | $CH_2O$, $C_2H_6$ | Richter et al. (2015), Fried et al. (2020) |
| Gwangju Institute of Science and Technology Korean Airborne Cavity Enhances Spectrometer (K-ACES) | CHOCHO | Min et al. (2016), D. Kim et al. (2022) |

| | | |
|---|---|---|
| NCAR CCD Actinic Flux Spectroradiometers (CAFS) | j-values | Shetter & Müller (1999) |
| Georgia Institute of Technology Chemical Ionization Mass Spectrometer (GT) | $SO_2$, PAN, PPN, APAN, PBzN | Kim et al. (2007), Lee et al. (2022) |
| University of Colorado, Boulder, High-Resolution Time-of-Flight Aerosol Mass Spectrometer | $pNO_3$ | Nault et al. (2018), Day et al. (2022) |
| NCAR 4-Channel Chemiluminescence Instrument (NCAR) | NO, $NO_2$, $O_3$, $NO_y$ | Weinheimer et al. (1994) |
| California Institute of Technology Chemical Ionization Mass Spectrometer (CIT) | Butene Hydroxynitrates, Butadiene Hydroxnitrates, Ethene Hydroxynitrates, Ethanal Nitrate, Isoprene Hydroxynitrates, Propene Hydroxynitrates, Propanal Nitrate, $CH_3OOH$, Peroxyacetic Acid, $HNO_3$, Hydroxyacetone, $H_2O_2$ | Crounse et al. (2006), Teng et al. (2015) |
| University of Oslo Proton Transfer Reaction Time-of-Flight Mass Spectrometer (PTR-MS) | Methanol, Acetaldehyde, Acetone+Propanal, Isoprene, MVK+MACR+ISOPOOH, Benzene, Toluene, C8-alkylbenzenes, Monoterpenes, MEK | Müller et al. (2014) |
| NSRC Meteorological and Geographical Data | Latitude, Longitude, Altitude, Temperature, Pressure | Crawford et al. (2021) |

1259

## Figures

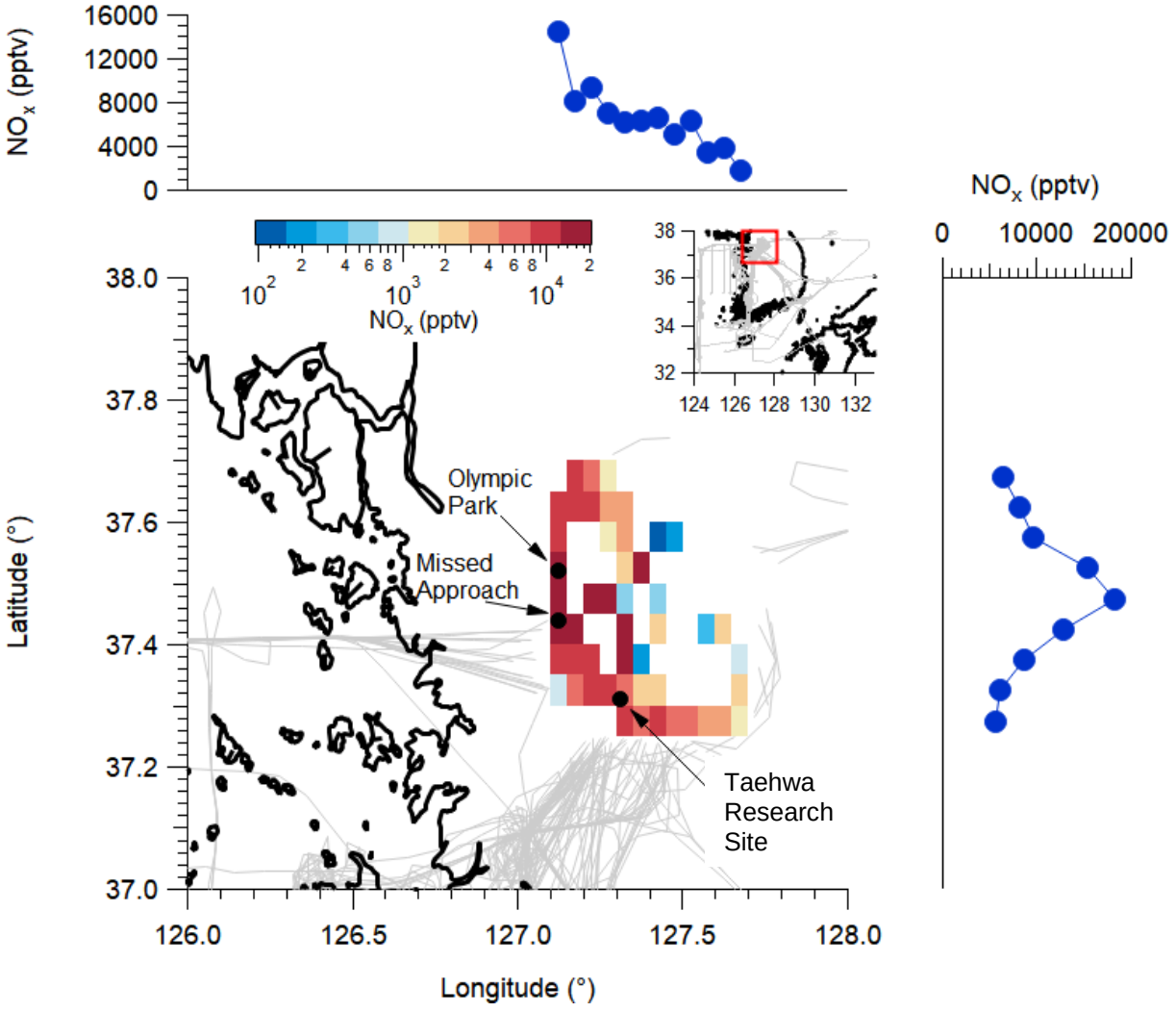


**Figure 1.** Binned $NO_x$ mixing ratios observed on the NASA DC-8 during the KORUS-AQ campaign. Note, the color bar scale is logarithmic. The binning is along the flight paths of the NASA DC-8 for any observations collected below 2.0 km and after 11:00 local time. The rest of the NASA DC-8 flight paths not included in the analysis are shown in grey. Three key areas from KORUS-AQ are highlighted—the Olympic Park ground site, the airfield where the NASA DC-8 conducted routine missed approaches, and the Taehwa Research ground site. The histograms above and to the left are the distribution of $NO_x$ mixing ratios longitudinally and latitudinally, respectively.

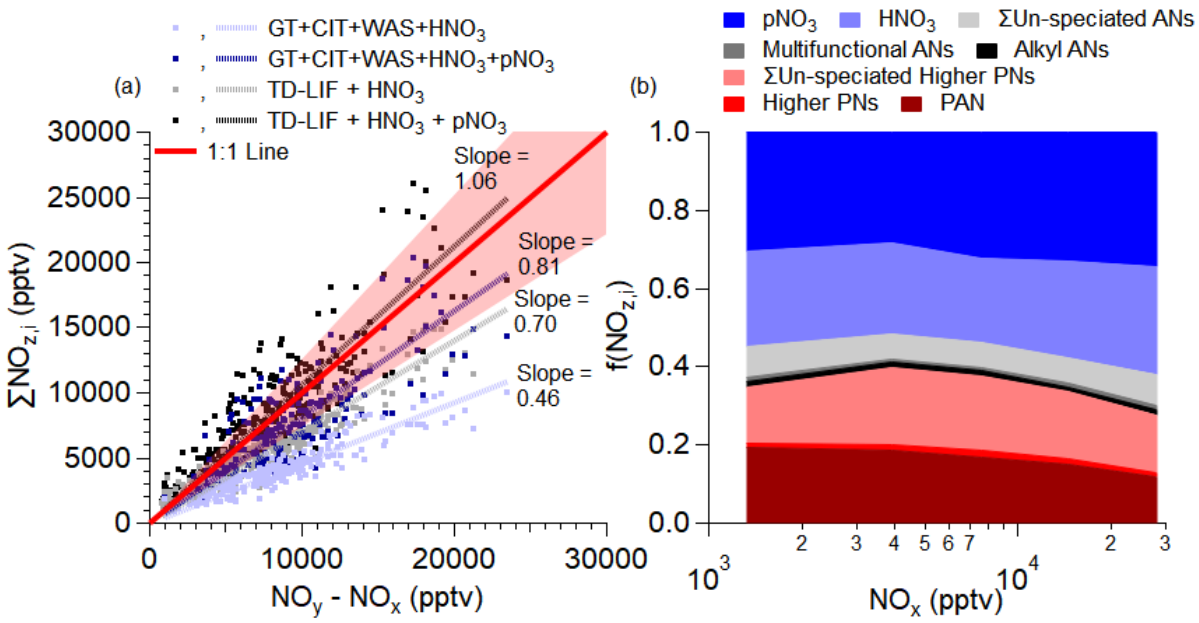


1270

1271 **Figure 2.** (a) Scatter plot of the summation of individual $NO_z$ ($NO_z$ is higher oxide $NO_x$ products)
1272 measured by GT, CIT, WAS, TD-LIF, and AMS versus $NO_z$ measured by difference between $NO_y$
1273 and $NO_x$ (see Table 2 for compounds measured by each instrument). $NO_x$ is NO measured by
1274 NCAR and $NO_2$ measured by LIF. The observations are for when the DC-8 was over the SMA.
1275 (b) Average contribution of measured speciated $NO_z$ over the SMA during KORUS-AQ versus
1276 $NO_x$. Higher PNs is PPN + APAN + PBZN. ΣUn-speciated PNs is total peroxnitrates from TD-
1277 LIF minus total measurement from GT. Alkyl $RONO_2$ is the total small alkyl nitrate measurements
1278 from WAS. Multifunctional $RONO_2$ is the total measurements from CIT. ΣUn-speciated ANs is
1279 the total alkyl nitrates from TD-LIF minus total $RONO_2$ from CIT and WAS.

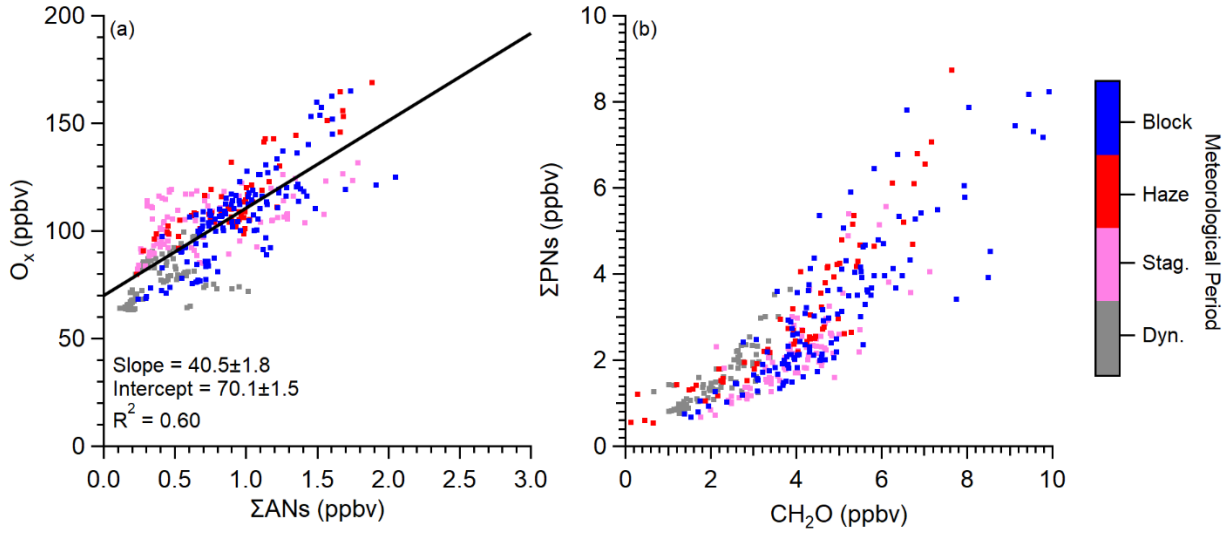


**Figure 3.** Scatter plot of (a) $O_x$ versus ΣANs and (b) ΣPNs versus formaldehyde ($CH_2O$) over SMA (see Figure 1 for area studied). Data is colored by meteorological periods discussed in Peterson et al. (2019). Data plotted here is after 11:00 am LT to minimize impact of growing boundary layer and nocturnal residual layer mixing. The curvature in (b) is further explored in Figure S9. Eq. 8, 9, and 11 is used to convert the slope in (a) into $\alpha_{eff}$. The units of the slope are ppbv $ppbv^{-1}$.

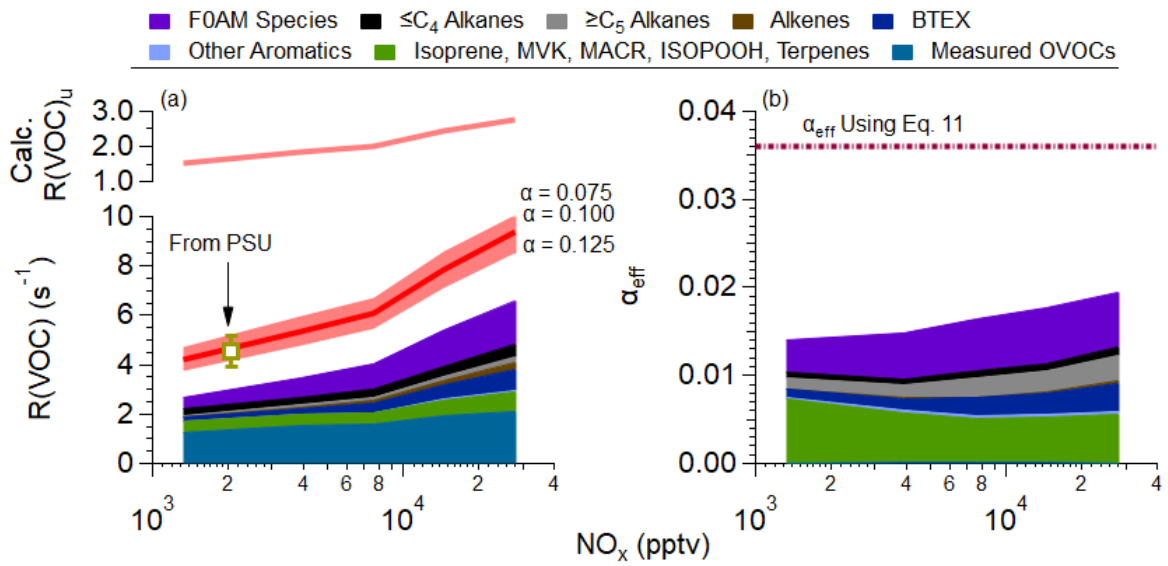


**Figure 4.** (a) Upper panel is the binned calculated (calc.) unmeasured VOC reactivity ($R(VOC)_u$). Note, unmeasured is for any species not measured on DC-8 or constrained by F0AM and is calculated using Eq. 13. Lower panel is binned VOC reactivity versus $NO_x$ observed over SMA during KORUS-AQ (see Figure 1 for the area studied). The measured observed R(VOC), labeled as "From PSU", where PSU is Pennsylvania State University, is the VOC reactivity calculated from the measured total OH reactivity with inorganic OH reactivity removed. As discussed in Brune et al. (2022), the OH reactivity has interferences at high $NO_x$ mixing ratios. The error bar is the uncertainty in the OH reactivity measurement (Brune et al., 2022). The red line represents the calculated unmeasured R(VOC), using Eq. 11, with an assumed $\alpha = 0.10$. The shaded area represents different calculated unmeasured R(VOC), assuming different $\alpha$ for the unmeasured R(VOC) (see Eq. 11). (b) The calculated effective $\alpha$ from observations versus $NO_x$. The dashed purple line is the effective $\alpha$ estimated from Eq. 11, using the slope from Figure 3a. For both (a) and (b), the colored stacked data is the calculated VOC reactivity (a) and weighted effective $\alpha$ (b). The values from (b) are calculated using Eq. 11. Finally, for both (a) and (b), F0AM species is the reactivity for compounds not measured on the DC-8 predicted by F0AM with an estimated $\alpha = 0.05$. The associated uncertainty in using different $\alpha$ for the F0AM predicted reactivity is explored in Figure S5.

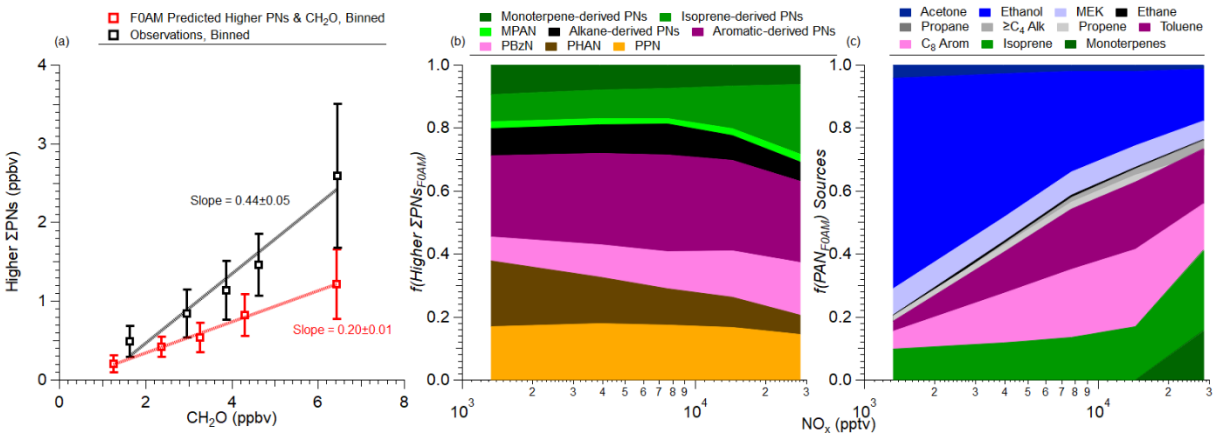


1305

1306 **Figure 5.** (a) Scatter plot of binned higher ΣPNs calculated using F0AM (red) or binned higher
1307 ΣPNs from observations (black) versus formaldehyde ($CH_2O$). Slopes shown are ODR fits to the
1308 binned data. PPN and PAN were constrained by observations for F0AM while all the other higher
1309 PNs were not constrained (b) Fractional contribution of the higher PNs predicted from F0AM
1310 versus $NO_x$. (c) Fractional contribution of different precursors to PAN, predicted by F0AM versus
1311 $NO_x$. For both (b) and (c), Alk is all alkanes, Arom is all aromatics, and ≥$C_4$ Alk is all alkanes with
1312 4 or more carbons. See Figure S10 for comparison of F0AM.

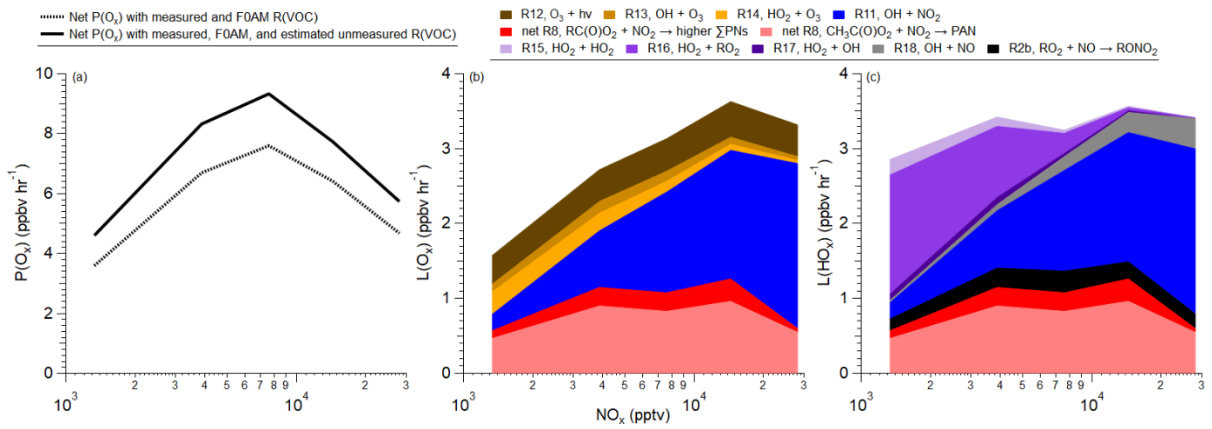


**Figure 6.** (a) Net $O_x$ ($O_3$ + $NO_2$) production (see Eq. 1 and 2) predicted for SMA using measured and F0AM R(VOC) (dashed) or total R(VOC) (solid), from Figure 4a, versus $NO_x$. (b) Contribution of different reactions to the total $O_x$ loss versus $NO_x$. (c) Contribution of different reactions to total $HO_x$ ($HO_x$ = OH + $HO_2$ + $RO_2$ + $R(O)O_2$) loss versus $NO_x$. The predicted $RO_2$ comes from the total VOC reactivity calculated in Figure 4a assuming steady-state (Eq. 7), and $HO_2$ the acyl peroxy radicals are from F0AM results. Note for both (b) and (c), net $RC(O)O_2$ + $NO_2$ and net $CH_3C(O)O_2$ + $NO_2$ are described in Eq. 3. Radical reactions contributing < 1% to the $L(O_x)$ or $L(HO_x)$ are not included. Also note that F0AM $HO_2$, $CH_3C(O)O_2^{\cdot}$, $R(O)O_2^{\cdot}$, and F0AM secondary products are used here along with observations.

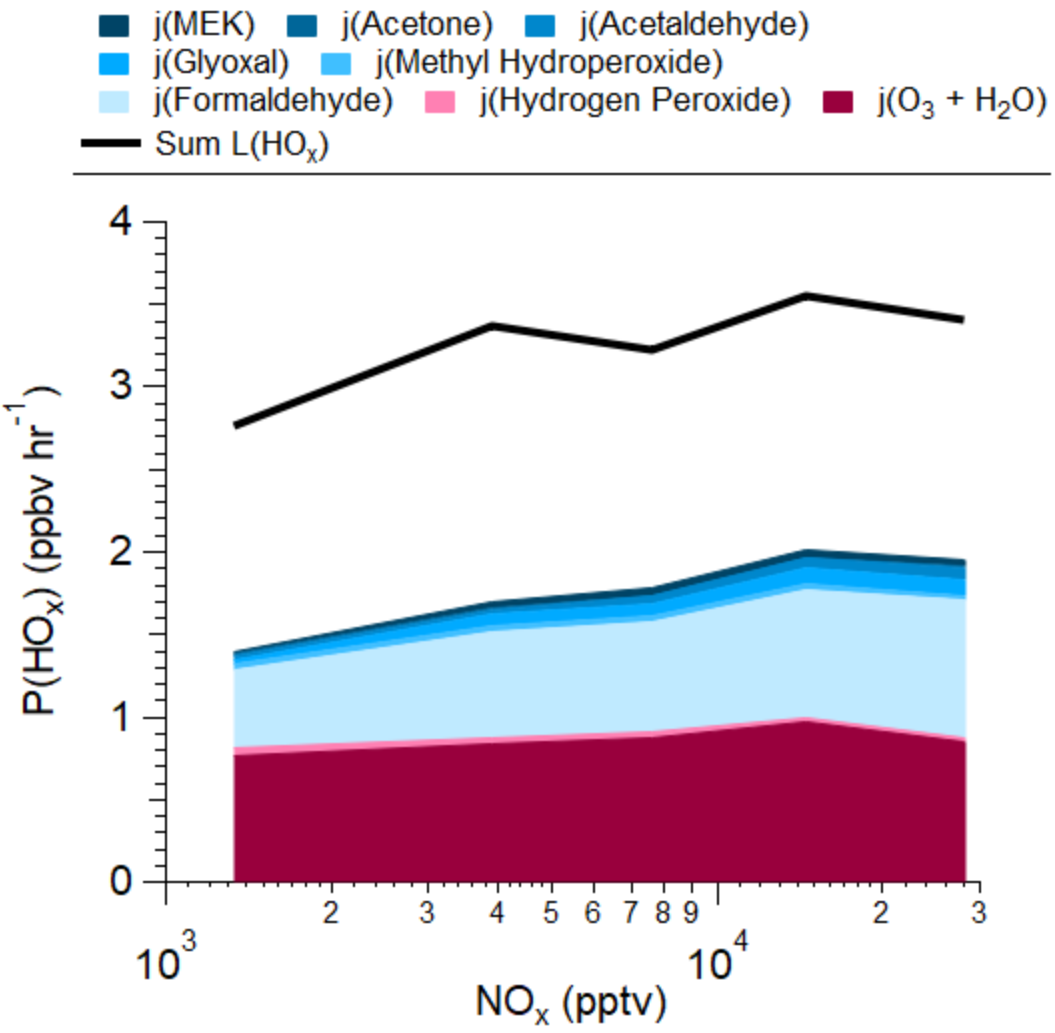


1323

1324 **Figure 7.** Calculated $HO_x$ production from observations (colored stack) compared with the
1325 calculated $HO_x$ loss from Figure 6c over the SMA during KORUS-AQ.